REPORT DOCUMENTATION PAGE	Form Approved OMB No. 0704-0188

1. AGENCY USE ONLY *(Leave blank)*	2. REPORT DATE	3. REPORT TYPE AND DATES COVERED
	20.Jan.99	THESIS

4. TITLE AND SUBTITLE
MOISTURE ANALYSIS OF A TYPE I CLOUD-TOPPED BOUNDRY LAYER FROM DOPPLER RADAR AND RAWINSONDE OBSERVATIONS

5. FUNDING NUMBERS

6. AUTHOR(S)
CAPT DREHER JOHN P

7. PERFORMING ORGANIZATION NAME(S) AND ADDRESS(ES)
CREIGHTON UNIVERSITY

8. PERFORMING ORGANIZATION REPORT NUMBER

9. SPONSORING/MONITORING AGENCY NAME(S) AND ADDRESS(ES)
THE DEPARTMENT OF THE AIR FORCE
AFIT/CIA, BLDG 125
2950 P STREET
WPAFB OH 45433

10. SPONSORING/MONITORING AGENCY REPORT NUMBER
FY99-48

11. SUPPLEMENTARY NOTES

12a. DISTRIBUTION AVAILABILITY STATEMENT
Unlimited distribution
In Accordance With AFI 35-205/AFIT Sup 1

12b. DISTRIBUTION CODE

13. ABSTRACT *(Maximum 200 words)*

14. SUBJECT TERMS	15. NUMBER OF PAGES 49
	16. PRICE CODE

17. SECURITY CLASSIFICATION OF REPORT	18. SECURITY CLASSIFICATION OF THIS PAGE	19. SECURITY CLASSIFICATION OF ABSTRACT	20. LIMITATION OF ABSTRACT

Standard Form 298 (Rev. 2-89) (EG)
Prescribed by ANSI Std. 239.18
Designed using Perform Pro, WHS/DIOR, Oct 94

MOISTURE ANALYSIS OF A TYPE I CLOUD-TOPPED BOUNDARY LAYER FROM DOPPLER RADAR AND RAWINSONDE OBSERVATIONS

BY

JOHN P. DREHER, MAJOR, USAF

A THESIS

Submitted to the faculty of the Graduate School of

Creighton University in Partial Fulfillment of

the Requirements for the degree of Master of

Science in the Department of Atmospheric Sciences

Omaha, NE December, 1998

ABSTRACT

Moisture data from radar and rawinsonde observations during three lake effect snow events are analyzed to determine entrainment rates. Gathered during the winter of 1990, the data is a sub-set from the Lake Ontario Winter Storms (LOWS) Project, which deployed a mesoscale network of sensors. Doppler wind profiler signal-to-noise ratio (SNR) data is used to derive humidity structure function parameter (C_q^2) time-height series analysis, which is then compared to rawinsonde specific humidity (q) plots. Visual comparison of $\log(C_q^2)$ and q analysis indicated a strongly positive correlation. Radar-derived humidity analysis is used to estimate the depth of the Type I, cloud-topped boundary layer (CTBL), which corresponded well with results from LOWS rawinsonde data. Calculations of the contribution of (C_q^2) to the refractive index structure parameter (C_n^2) showed the humidity correction factor (α_r^2) to range from 1.03 to 1.04 within the CTBL, consistent with previous findings for Type II CTBLs. A comparison of entrainment rates, computed via two different methods, were in agreement.

Table of Contents

Tables

Figures

1. Introduction

Much of the theory behind radar observations in clear air comes from turbulence studies. Researchers in the 1940s through the early 1960s laid the foundation for the stoichaotic description of the atmospheric turbulence. From the result, clear air radar observation theory was refined in the late 1960s through the early 1990s. Operational applications rapidly followed theoretical developments. It was discovered early that the turbulent mixing of the atmosphere causes gradients of temperature, moisture, and pressure, and hence gradient of the refractive index. Radars of sufficient wavelength are capable of sensing these refractive index inhomogeneities, as they are almost always present within the turbulent atmosphere below the stratopause.

This thesis presents a study of the moisture profiles within a Type I cloud-topped boundary layer (CTBL) using wind profiler and rawinsonde data. It closely mirrors the study of the moisture structure of a Type II CTBL conducted by White et al. (1991) off Southern California. A Type II CTBL is defined as a convective boundary layer primarily driven by radiative cooling at cloud top (with nearly thermal equilibrium at the sea surface). The Type I CTBL differs in that it is driven largely by heating from below as cold air moves over relatively warm water (Agee, 1990). The data utilized comes from the Lake Ontario Winter Storms (LOWS) Project, a detailed investigation of mesoscale motions within Lake Ontario lake-effect snowstorms (LESS) during the winter of 1990 (Reinking et al., 1993). In the LESS environment, surface fluxes of moisture and temperature drive convection that lead to localized snowfall events. The LOWS data set includes in-situ measurements of the planetary boundary layer using rawinsondes, instrument towers, and surface observations to increase knowledge of dynamic motions and meteorological variables within the mesoscale environment. Doppler radar wind proflilers were also key remote-sensing tools, having the advantage of increased spacial and

temporal sensing. From the radar reflectivity and spectrum width data, important meteorological information can be derived. Reflectivity data caused by refractive index irregularities in clear air (Bragg scattering) will be used in this study to derive entrainment rates. These rates will be analyzed in regards to boundary layer growth at one wind profiler site. Comparisons will be made with the results of Type II CTBL studies and with previous conclusions from the 1990 LOWS study.

2. Data

Lake Ontario LESS events are unique. There is a well defined snowbelt as a result of the lake's length and orientation to the prevailing winds, and due to the orographic enhancement effects of rising terrain on the leeward (in this case eastern) portion of the lake. Single band snow storms frequent Lake Ontario and Lake Erie, remaining infrequent events on the other Great Lakes. However, Lake Ontario is much deeper than Lake Erie, helping to maintain large areas of ice-free lake surface and potential for heat and moisture fluxes into the boundary layer throughout most winters. On the other hand, Lake Erie's LESS season is considerably shorter, as ice often covers most of the lake surface by mid-winter.

2.1 Lake-effect Snowstorms

Primarily a mesoscale phenomena, lake-effect storms are however a complex interaction of synoptic scale, mesoscale, and microscale. Lake-effect snow events develop when the atmosphere is destabilized as post-frontal Arctic or polar air passes over a relatively warm lake surface. This causes a positive flux of heat and moisture into the atmosphere producing convection and thickening of the boundary layer through entrainment. Single or multiple parallel bands of precipitation form which can produce localized heavy snowfalls. Wind direction plays an important role in determining band types and location. Advection length-wise along the lake tends to produce intense single bands, while all other wind directions produce weaker multiple

bands. Additionally, orography serves to enhance vertical velocities and increase snowfall amounts. The primary and secondary factors which influence lake-effect snow development are listed in Table 1.

Primary Factors	Secondary Factors Related to Primary	
Strong flow of Arctic air across a relatively warm lake	850 mb temperature of -10° for lake water ≥ 2°	- 850 mb temperature of -12° for lake water < 2°
Relatively long fetch across lake	40 miles with PVA and 850 temperature ≤ -5°	- 100 miles otherwise
Positive vorticity advection	NVA and rising surface pressure are deterrents to snow production	
Frictional and thermal convergence		
Orographic lifting		
Latent heat release		

Table 1. Primary LESS and secondary related factors. Adapted from Penc (1995).

2.1.1 Lake-effect Storm Types

Single or double banded storms form parallel to the winds aloft and aligned along the long axis of the lake due to organized convergent flows which serve to force convection into the center of the lake. Typically, storm dimensions are 2-20 km wide and 50-200 km long, with cloud tops to 4 km (Peace and Sykes, 1996). The single banded storm is the most intense of lake effect snow storms, capable of producing heavy localized snowfalls.

Multiple banded storms occur when the winds are aligned along the short axis of the lake. Normally these storms are 5-80 km long with aspect ratios ranging from 5:1 to 12:1 (Peace and Sykes, 1996). The boundary layer remains relative shallow with 1-2 km cloud tops. The bands drift with the wind at small angles to the mean wind, generating widespread, but light,

precipitation.

2.1.2 Thermal Instability Indicators

Operationally, the Collier index is used to determine potential for and severity of lake effect snow events, measuring the degree of thermal instability between the lake surface and the lower troposphere (Niziol, 1987). Additionally, it has been noted that a deepening of the boundary layer is almost always associated with the events (Penc, 1995). Boundary layer depths of 3-4 km are seen with the most severe storms (Niziol, 1987). Numerical modeling studies have shown heating and moistening of the atmosphere are responsible for increasing boundary layer depth by hundreds of meters (Lavoie, 1972). During LOWS, changes in the height, as well as the strength of the capping inversion were indicated to be the most important factors in lake effect snow band intensity. LOWS researchers found the intensity of the convection was more closely related to the depth of the convective mixed layer than to the degree of lower atmospheric thermal instability. The greatest snowfalls occurred during single band storms on 12 and 14 January 1990, where CBL heights ranged between 2.5 and 4 km (Penc, 1995).

2.2 Lake Ontario Winter Storms (LOWS)

The Lake Ontario Winter Storms project was conducted from 5 January to 1 March 1990 to demonstrate and evaluate mesoscale observation and forecasting techniques applicable to location-specific lake-effect storms and freezing rain. In order to resolve mesoscale features, an array of six specialized remote sensors (a dual-polarization short wavelength radar, microwave radiometer, radio acoustic sounding system, and three wind profilers) were deployed, as well as a full compliment of project-specific and standard meteorological observing systems. Researcher from various universities, government agencies, and private consulting firms participated in the project as summarized in Reinking et. al. (1993).

2.2.1 Meteorological Conditions

Due to warmer than normal air temperatures during LOWS, occurrences of lake-effect snow events were below normal. To establish the scope of this study, lake-effect snow data sets were analyzed for the single band storms of 11-13 January and 14 January, and the multiple band storm events of 25-26 February and 27 February - 1 March. This data encompassed the four "marginal" or greater episodes, as described by Penc (1995), and included sub-hourly radar and rawinsonde data collected during LOWS intensive observation periods (IOPs).

2.2.2 11-14 January 1990

After the passage of an occluded front between 2100 and 2200 UTC on 11 January, the synoptic situation was favorable for development of lake-effect snow. During 12 January, an intense, 980 mb surface low, approximately 500 km north of Lake Ontario, tracked east producing west to southwest flow along the major axis of the lake from 0000 to 1800 UTC. Aloft at 500 mb, a broad trough also produced westerly flow. Surface air temperatures ranged from -1°C to -3° with the Collier Index remaining in the conditional category. Deep cold air advection along with moderated positive vorticity advection (PVA) produced destabilization that supported development of a stationary single snowband over the lake. Four snowbands formed over the center portion of the lake beginning around 0130 UTC, with the final snowband dissipating around 1700 UTC. The snowbands formed over the warmest part of the lake (near 4°) and moved inland over the eastern shores of the lake producing up to 80 cm snowfall amounts.

At 0000 UTC on 14 January, the surface low had moved to a position off the Canadian maritimes and was deepening, while a significant shortwave trough stretched from James Bay toward Minnesota. Surface air temperatures ranged from -13° northwest of the lake to -6° to -9° southeast of the lake. The Collier index remained in the conditional category, but approached

moderate. The approaching shortwave trough and broadening longwave trough led to increased westerly flow and longer fetch over Lake Ontario. Snowfall with this event was confined to the southeast shore of the lake with accumulations up to 15 cm. Visibilities dropped to zero at Oswego, NY at 0600 UTC, with occasional thunder and lightning.

Of note is the possibility that some of the snowfall during these two events may be attributed to synoptic forcings, as well as to lake-effect snow conditions. The resulting snowfall may be referred to as lake-enhanced snow. However, for the scope of this study, only the lake-effect factors will be considered.

2.2.3 25 -26 February 1990

Multiple lake-effect snowbands occurred after a west-east oriented surface trough passed over the southern portion of the lake approximately 1200 UTC on 25 February. Snow fell over the entire region just prior to the trough passage, which was then followed by light lake-effect snowfall for a 12 hour period over the southeastern portion of the lake. A tight pressure gradient providing strong northwest winds after the passage of the trough advected in very cold surface temperatures (-20 to -26°C). Despite a short fetch, thermal instability was great enough produce moderate to extreme Collier indices. By 1500 UTC, multiple north-south bands were seen over the southeastern portion of the lake and with a moderate burst of snowfall at the North Rose radar site. As the boundary layer winds continued backing, snow band orientation changed through northwest-southeast, and eventually northeast-southwest by 0300 UTC on 26 February. Strong surface to 850 mb ridging was evident by 0000 UTC on 26 February causing rapid slackening in the pressure gradient and decreasing cold air advection. By 1200 UTC, only a solitary weak dissipating snow band remained. In general, the lake-effect snowfall totals were very light in this short-lived event. Only 4 cm accumulated at North Rose, directly attributed to lake-effects.

2.2.4 27 February - 1 March 1990

A cold front approached on 27 February and passed over the lake around 0000 UTC on 28 February, after which multiple snowbands developed. At 1200 UTC on 28 February there was high pressure centered over the upper Midwest producing northwesterly flow over the Great Lakes region. Surface temperatures ranged from -12° north of the lake to -8° southeast of the lake while 850 temperatures were -17° to -18°, leading to a moderate Collier index. With a 500mb trough providing westerly flow aloft, little directional shear was present in the troposphere. By 1400 UTC on 28 February, radar showed multiple snowbands extending inland on the southeastern shore of Lake Ontario. By 1700 UTC radar echoes ceased. More weak banded echoes resumed at 2200 UTC, then dissipated by 0400 UTC on 01 March. Snowfall along the southeastern portion of the lake was > 5cm with a maximum of 15cm (Penc, 1995).

2.3 Radar Specifications and Siting

The radar data analyzed was retrieved at North Rose, NY, on the southeast corner of Lake Ontario approximately 5 km inland from the lake shore. From this location, measurements could be taken within and near single and multiple banded snow events. Multiple band snow events frequent the North Rose site, whereas single band events often occur farther north, allowing the North Rose site to provide measurements of parameters associated land-to-lake convergence areas. The data was recorded on magnetic media by the operators of the 404 MHz UHF Doppler wind profiler provided by Penn State University. This profiler used a three beam system with two orthogonal off zenith and one vertical. Data archived included returned signal power, wind velocity, and wind spectral width, which are the zeroth, first, and second spectral moments, respectively. Measurements were made in high mode (east, north beams) followed by low mode (vertical, east, and north beam) every 3 1/2 minutes. During intensive observation periods, the sub-hourly information was recorded for all range gates (Penc, 1992). For the scope

of this study, the sub-hourly signal to noise ratio (SNR) data from the low mode vertical beam was used.

2.3.1 Data Processing and Quality Control

In order to accurately calculate atmospheric variables from radar reflectivity data, the radar must be properly calibrated. The Penn State 404 MHz wind profiler was calibrated at Otis

Radar Characteristics	
Frequency	404.37 MHz
Wavelength	0.742m
Maximum bandwidth	2 MHz
Peak power	9.0 kW
Duty cycle	<25%
Antenna Aperture	47.0 m^2
Antenna pointing	zenith, 14.5°off-zenith to north and east
Antenna type	Fixed-phased array of collinear, coaxial dipoles
Antenna element spacing	0.3125 m
One-way beamwidth	~ 7°
System noise temperature	~ 100°K
Operating Parameters	
Vertical Data Processing	
Pulse width (τ)	1 μs
Pulse repetition period	100 μs
Average power	80 W
Time domain averaging (n_c)	200 pulses
Spectral averaging (n_s)	8 spectra
Maximum radial velocity	± 9.27 ms^{-1}
Spectral resolution (k_3)	0.290 ms^{-1}
Height Sampling	
First height	0.40 km
Height spacing	100 m
Number of heights	22

Table 2. Radar characteristics and operating parameters for the Penn State 404 MHz wind profiler deployed at North Rose, NY. (Penc, 1992)

Air Force Base in southeastern Massachusettes, 11 months before the LOWS project began. Calibration used data from an aircraft-mounted Lyman-α hygrometric sensor that was compared with radar-deduced humidity profiles. This radar is the same as used by White et al (1991) in the study of humidity profiles in a Type II CTBL.

Signal processing is largely based on techniques developed at the NOAA Wave Propagation Laboratory (Staunch et al., 1984). Before archival, the raw data is filtered using a series of steps. First is a coherent integration or time domain averaging, which reduces the amplitude of components outside the maximum frequency measured. Next is a spectral or incoherent averaging which improves the detection of the spectral peak by smoothing out the noise floor. Then, a low-pass filter is employed which rejects data below -18 dB. In addition to the aforementioned filtering, data quality control was achieved by periodic monitoring of the SNR and comparison with collocated rawinsondes.

3. Remote Sensing Theory

Radar returns in clear air result from inhomogeneities in the refractive index caused by turbulence. The intensity of the return radar caused by the inhomogeneities can be used to derive temperature and humidity values. In the study of propagation of electromagnetic energy through a turbulent atmosphere, the refractive index structure parameter (C_n^2) is the key to analyzing returned radar backscatter power (P_r) in terms of the refractive index (n), temperature (T), and moisture (specific humidity, q) analysis. It has been shown that the returned backscatter power received by the radar is proportional to the refractive-index structure parameter (Van Zandt et al, 1978). The theory behind this remote sensing is presented.

3.1 Turbulence parameters

Following Fairall (1991), consider some atmospheric variable $X(r)$ as a function of location r. The structure function $D_x(d)$ of X is defined by

$$D_x(d) = [X(r+d) - X(r)]^2 \quad (3.1)$$

where d denotes a separation distance and the overbar denotes an ensemble average. Assuming isotropic turbulent fluctuations within the inertial subrange, the structure function parameter can also be expressed in the 2/3-law form as (Tatarski, 1961)

$$C_x^2 = D_x(d) / d^{2/3} \quad (3.2)$$

For the refractive index (n)

$$D_n(d) = [n'(r+d) - n'(r)]^2 = C_n^2 \, d^{2/3} \quad (3.3)$$

where n' indicates perturbations in the spatial mean of the refractive index.

3.2 The Radar Equation

The radar equation can be expressed as a relation of backscattered power at the radar antenna P_r to the average reflectivity per unit volume η of the target

$$P_r = P_t \, G^2 \lambda^2 \theta^2 \, h\eta / (1024 \pi^2 (\ln 2) \, r^2) \quad (3.4)$$

where P_t is the radar transmitted power, G is antenna gain, λ is the radar wavelength, θ is the radar beamwidth (full width at half maximum) in radians, h is the transmitted pulse length, r is the range to the target. From the radar equation a value of η can be obtained, since P_r can be measured and the remainder of the radar equation parameters known. Again, assuming the refractive index fluctuations are a result of isotropic turbulence in the inertial subrange and of length scale within $\lambda/2$, the reflectivity of clear air can be expressed as (Ottersten, 1969)

$$\eta = 0.38 C_n^2 \lambda^{-1/3} \quad (3.5)$$

From this expression, it can be observed that for radar wavelengths of 10 cm or more, the structure constant C_n^2 is directly proportional to the radar reflectivity η. Radars of shorter wavelengths are sensitive to smaller scales, and therefore may be observing contributions of dissipation by molecular diffusion, depending on the energy dissipation rate (Ottersten, 1969).

3.3 Humidity Structure Function Parameter (C_q^2)

The radio refractive index is a function of temperature, humidity, and air pressure, where within the PBL, the effects of air pressure can be ignored. Refractive index fluctuations can be expressed as a linear combination of fluctuation in temperature and humidity. Equations (3.1) and (3.2) were used to obtain the scalar structure function parameters expressed as

$$C_n^2 = (6 \times 10^{-4} P/T^2)^2 C_q^2 \alpha_r^2 \quad (3.6)$$

where C_q^2 is the humidity structure function parameter (Wesely, 1976) and

$$\alpha_r^2 = 1 - 2ar_{Tq}C_T/C_q + a^2 C_T^2/C_q^2 \text{ and} \quad (3.7)$$

$$r_{Tq} = C_{Tq} / (C_T/C_q). \quad (3.8)$$

In these expressions, the quantity $(\alpha_r^2 - 1)$ gives the deviations from the pure moisture dominated C_n^2. C_T^2 is the temperature structure function parameter , r_{Tq} is the temperature-moisture correlation coefficient, and

$$a = 0.13(1 + 15.4q/T) \quad (3.9)$$

(Fairall 1991). Contributions of C_T^2 and C_q^2 to C_n^2 were investigated by Wesely (1976). Within the lower troposphere, he found C_q^2 dominated. VanZandt (1978) also extended this result above the boundary layer to a few kilometers of the troposphere based on a rawinsonde, radar, and model data correlation study. Above a few kilometers and into the ionosphere, C_T^2 is the primary contributor to C_n^2. Exceptions within the PBL for C_q^2 domination may exist in extremely dry and strongly convective atmospheres. Therefore, $\alpha_r^2 \simeq 1$ for most marine and continental PBLs in the tropics and mid-latitudes.

Following White et. al (1991), after rearranging (2.6) in terms of C_q^2, substituting (2.5) into (2.6), and where $T = 268^o$, $P \simeq P_0 e^{(-z/H)}$ is the pressure in millibars, z is the altitude in kilometers, $P_0 = 1000$ mb, and $H = 8$ km yields

$$C_q^2 = (1.66 \times 10^3 T^2/P)^2 \alpha_r^{-2} (\eta/0.38) \lambda^{-1/3}. \quad (3.10)$$

From this equation, the turbulent humidity structure of the atmosphere can be calculated.

In order to relate η to a quantity measured by the Doppler radar we use the reflectivity equation given by VanZandt et al. (1978):

$$\eta = 9\pi c k_0 B(\alpha T_c + T_{rx})(R^2/\Delta R^2)(SNR)[2\alpha^2 P_t F_r A_e \cos(\chi)]^{-1} \quad (3.11)$$

where $c = 2.998 \times 10^8$ m s^{-1} is the speed of light in a vacuum, $k_0 = 1.3803 \times 10^{-23}$ J mol^{-1} K^{-1} is Boltzmann's constant, R is the range, and the remaining parameters are listed in Table 3.

Symbol	Parameter	Value
A_e	Effective antenna area (one section equal to geometric area	47.0 m^2
α	Efficiency of radar antenna and transmission line	0.10
P_t	Peak pulse power	9.0 kw
χ	Off vertical beam axis angle	14.5°
T_{rx}	Receiver noise temperature	100 K
T_c	Cosmic noise temperature	10-100 K
ΔR	Range resolution	149.9 m
F_r	Pulse repetition frequency	10kHz
B	Bandwidth of integrating filter	50.0 Hz

Table 3. Radar characteristics and signal processing parameters used in deriving the relationship between reflectivity and signal to noise ratio (SNR) for the Penn State 404 MHz wind profiler. (Penc, 1995)

Combining (2.10) with (2.11) and substituting values from Table 3 gives the form of the C_q^2 equation used in this study:

$$C_q^2 = 1.63 \times 10^{-15}(T^2/P)^2 \alpha_r^{-2} R^2 10^{SNR/10} \quad (2.12)$$

where SNR is now conveniently in decibels (dB), as it was recorded during the four LOWS IOPs used in this study.

4. Data Analysis Procedures

A number of steps were taken organize the raw radar and rawinsonde data into a format

suitable for computational and visual analysis. In order to compute entrainment, C_q^2 values had to be derived from the raw radar data. To compute moisture/temperature contributions to C_q^2, α_r^2 must be derived from rawinsonde data. For convenience sake, personal computer-based display and spreadsheet software were used.

4.1 Radar Data

Originally, the raw radar data from the North Rose wind profiler was stored on magnetic media as individual files sorted by day. Most of the files contained an entire day's data (> 4 Mb) with information from each beam (east, north, and vertical) and mode (low, high) that was recorded every three minutes (sub-hourly data). The sub-hourly data incorporated raw spectra and moments tables, consisting of the following parameters in tabular form by range gate: horizontal velocity, returned power, noise, signal-to-noise ratio (SNR), and spectral width. In this boundary layer growth study, only the SNR fields from the moments tables for the vertical beam were required for computations and analysis. Additionally, the higher resolution low mode data was desired as the boundary layers in the study remained below the low mode top range gate (2600m). Since only a small portion of the copious raw radar data was required, a C program was written to parse and store the applicable data on a desktop PC. Also, the output of the DOS-based executable needed to be in a grid format compatible with SURFER, a mathematical grid manipulation and isoplething software package.

Equation (3.12) was applied to the original SNR ratio grids to obtain C_q^2 grids, from which $\log(C_q^2)$ grids were calculated. Next a 2, 1 time-height matrix smoothing was applied to the $\log(C_q^2)$ grids and then plotted.

4.2 Rawinsonde Data

Raw rawinsonde data was used to determine temperature and moisture contributions to C_n^2 and combined with $\log(C_q^2)$ values to obtain entrainment velocities (w_e). The original ASCII

files were imported into MS EXCEL spreadsheets, then meteorological parameters were derived. To make time-height series spreadsheets, like parameters from individual soundings were combined. Sparse linear data interpolation was necessary to maintain consistent height data, however because the resolution of the sounding data (~50m) is significantly better than the radar data in low mode (~150m), there should be little error injected into the entrainment computations.

The meteorological parameters were calculated from the original rawinsonde data as shown in Table 4, where RH is relative humidity, p is pressure (mb), p_o is surface pressure (mb), T is temperature ($^{\circ}C$):

specific humidity (q)	$q =. 037990516\ RH\ exp[\ (17.27\ T) / (T + 273) - 35.86)] / p$
potential temperature (θ)	$\theta = (T + 273)(p_o/p)^{.286}$
saturation vapor pressure (e_s)	$e_s = 6.1078\ exp[\ (17.27\ T) / (T + 273) - 35.86)]$
saturation mixing ratio (w_s)	$w_s = 0.622\ (e_s / (p - e_s))$
actual mixing ratio (w)	$w = w_s\ RH / 100$
virtual potential temperature (θ_v)	$\theta_v = \theta(1 + 0.61\ w)$

Table 4. The meteorological parameters calculated from the original rawinsonde data and applicable equations.

4.3 Alpha (α_r^2) Calculations

To accurately assess the individual temperature and humidity structure parameter contributions, α_r^2 must be estimated using (3.12), as the quantity (α_r^2 -1) gives the deviation from pure moisture dominated C_n^2. It is generally agreed upon that α_r^2 is near unity in the non-convective PBL. However in the LOWS cases studied, the PBL is highly convective, therefore a detailed analysis was required using sounding data. From Burk (1981), we have a method for

determining relative contribution to C_n^2 using the following equation, which is another version of (3.7):

$$\alpha_r^2 = 1 - [(2A\epsilon/C) + (4\epsilon e/pT)][2.2 - 2.4Tr/3.9\rho r] + [(A\epsilon/C) + (2\epsilon e/pT)]^2[(0.5 - 2.6Tr + 1.4(Tr)^2)/(3.9(\rho r)^2)] \quad (4.1)$$

where A is a coefficient in microwave refractivity (77.6×10^{-6} K mb^{-1}), C is a coefficient in microwave refractivity (0.375 K^2 mb^{-1}), p is pressure (mb), T is absolute temperature, e is vapor pressure (mb), ϵ is the molecular weight of water/dry air (0.622), ρ is the density of air, $r = \Delta q/\Delta\theta_v$ across the interfacial layer. To obtain the changes of specific humidity and virtual potential temperature at a specific height, gradients were calculated from rawinsonde data using respective values immediately below and above the layer in question. All computations were accomplished on spreadsheets from which time-height series graphs were created, then imported to SURFER for analysis.

4.4 Entrainment Velocity (w_e) Calculations

Entrainment is the mixing down of less turbulent air into the PBL, thereby enhancing boundary layer growth. (Stull, 1988) The entrainment velocity is therefore one of the key parameters to evaluate interactions occurring in the inversion near the cloud tops. After applying the moisture deviation from (4.1) to C_q^2 values obtained from (3.12), entrainment values can be calculated following Wyngaard and LeMone (1980):

$$w_e = 6\,\Delta\theta_v\,\varepsilon^{1/3}\,C_q^2\,[11.2\,(\Delta q)^2\Gamma]^{-1} \quad (4.2)$$

evaluated at the middle of the interfacial layer where θ_v is the virtual temperature, Γ is the lapse rate of θ_v above the inversion, Δ denotes changes across inversion, ε is the rate of dissipation of turbulent kinematic energy for cloudy conditions (1.0×10^{-3} m^{2}s^{-3}). The base and the top of the inversion ware taken to be the span of the lowest temperature inversion identified in virtual temperature profiles and/or visual analysis of moisture profiles. Γ was calculated for the first 1000 m above the inversion.

5. Interpretation of Data

Entrainment of air from the free atmosphere into the convective boundary layer enables larger precipitation-producing convective eddies in the mixed layer. In order to obtain reliable estimations of the height of the convective boundary layer and entrainment velocitiy from the radar data, accurate moisture profiles were needed. According to the theory presented in section 2, the radar refractivity is proportional to gradients of moisture and temperature. It has previously been determined that in Type II CTBLs, the radar reflectivity of clear air is primarily dependent upon moisture contributions (Fairall, 1991). The humidity structure function parameter serves as a relative measure of these gradients of turbulent mixed moisture and can be calculated from radar reflectivity data. Since it is known that moisture generally decreases with height and the moisture gradients are largest at the top of the CTBL, time-height graphs of $\log(C_q^2)$ values can be used to monitor CTBL depths. In order to ensure this relationship is valid, either a parameterization concerning the contributions of moisture to the index of refraction must be made or a calculation from rawinsonde data. The radar humidity data has the temporal advantage of observations every 3 1/2 minutes, whereas rawinsondes were launched at various frequencies (1 to 5 per day). However, in the vertical, the rawinsonde's humidity data resolution was 50 m, compared with 150 m for the radar.

Signal-to-noise ratio (SNR) time-height series data appears in Figs. 1-4 for the 11 -14 January single band events and in Figs. 5-8 for the 25-26 February and 28 February - 1 March muliple band events. Figs. 1-8 show values of SNR generally decrease with height, with a few exceptions. One major exception is in Fig 3 for 13 January, where the radar malfunctioned for a short period around 1900 UTC. Without the known temperature and moisture contributions to the refractive index, other direct interpretations as related to convective boundary layer

features are premature. Therefore, the in-depth discussion of radar data will be later in this section.

5.1 Alpha (α_r^2) Calculations

As previously stated, the quantity (α_r^2 -1) gives the deviation from pure moisture dominated C_n^2. Studies of non-convective PBLs have shown α_r^2 near unity. Model studies have produced values for α_r^2 near unity for cloud-free convective boundary layers. According to Fairall (1990) there are three ways clouds change the radar refractivity potential of the boundary layer: an additional thermodynamic coupling between temperature and moisture results due to condensation processes, the entrainment rate is greatly enhanced by cloud-top radiative cooling, and cloud liquid water droplets provide an additional scattering mechanism for radar. Fairall states, based on simple physical reasoning, the results for α_r^2 are approximately valid for the entrainment-induced effects associated with clouds. Similar conclusions were reached in a modeling study of two maritime boundary layer cases even in the presence of clouds by Burk (1981).

The results of α_r^2 for the LOWS data are best shown by Fig. 9. Throughout the time frame, values for α_r^2 ranged from 1.02 to 1.04 within the boundary layer. Therefore, based on (3.6), contributions of C_q^2 to C_n^2 are 96 to 98 percent. Additionally, for modeling studies and calculations involving the refractive index structure parameter, an assumption of α_r^2 near unity will introduce very little error (< 4%). Of note in Fig. 9, as the boundary layer depth decreased under the effects of subsidence, α_r^2 showed increasing variability above the boundary layer. By visual inspection, this result appears to be directly correlated with the specific humidity vertical profile in Fig 10. However, these moisture gradients still have little effect on the overall contributions of C_q^2 to C_n^2 within the convective boundary layer.

5.2 Humidity Data

A visual comparison of specific humidity (Fig. 10) with $\log(C_q^2)$ for 11 - 14 January (Figs. 11-14) shows excellent correlation. Specifically, Fig. 10 at 2300 UTC on 11 January shows increased specific humidity at 600m, 1600m, and 2500m. Whereas, Fig. 11 shows increased $\log(C_q^2)$ values at 600m, 1600m, and 2200m. This corresponded with the passage of a surface front, after which lake-effect snow bands formed in the post-frontal environment. Cold front/trough passages were typified by moderately narrow uniform vertical $\log(C_q^2)$) fields. In Fig. 11, 1900-2100 UTC on 11 January, uniform vertical values of $\log(C_q^2)$ exceed -3.6 then rapidly transitioned to -4.5. Light snowfall in the pre-frontal environment was seen as high values (> -4.2) of $\log(C_q^2)$ with loose vertical gradients and a boundary layer depth of around 2200m. Three distinct snow bands are seen in Fig. 12 on 12 January, 0400-0800 UTC indicated by very narrow uniform vertical $\log(C_q^2)$) fields.

Continuing the visual comparison, Fig. 10 at 1600 UTC on 13 January indicates specific humidity increases at 1000-1200m, 1600-2000m, and 2250-2450m. Whereas, Fig. 13 shows increased $\log(C_q^2)$ values 1000-1300m, 1600-1800m, and 2200-2400m. In Fig. 14 on 14 January, the last snow band is seen around 0900 UTC, then frontal passage at 1400 UTC, with considerable drying of the atmospher thereafter. Fig. 15 depicts specific humidity for the 28 February, 1700 UTC sounding. While the change in specific humidity is nearly linear, closer inspection reveals decreases in the rate of change at 500-800m, 1250-1600m, 2250-2450m. Fig 16 shows a similar pattern, however visual correlation is not as prominent as in the previous examples.

5.3 Boundary Layer Heights

The depth of the boundary layer limits convective eddys and therefore the intensity of lake-effect snow events. From vertically pointed radars we can obtain moisture profile (time-

height series $\log(C_q^2)$) data that may be used to estimate boundary layer heights. Normally, atmospheric moisture content, and hence, C_q^2 decreases with height. However, sharp moisture gradients near the inversion cause local C_q^2 maximiums, from which depth of the boundary layer can be distinguished. For the most part, these features are easily recognized. As one might expect, the banded snow events that frequent the North Rose site can be seen as sharp changes in boundary layer depth.

The 25-26 February multiple snow band event exemplifies the approach to determining boundary layer heights. In Fig. 19 at around 0200 UTC, a rapidly moving "Alberta Clipper" was transitioning through the area producing widespread light snow. The boundary layer remained around 2300m until approximately 0800 UTC when cold dry air moved rapidly in behind the system as it exited. By 1200 UTC, the boundary layer depth was reduced to 1200m. Despite the short fetch due to northerly surface winds, convection was seen around 1630 UTC as the boundary layer quickly rose to 2300m when a lake-effect snow band moved over the radar site. At 2100 UTC the boundary layer dropped back to 1200m. Then the last snow band passed overhead 0230-0400 UTC, after which the boundary layer rapidly deflated as strong high pressure and subsidence moved in. This event left 4 cm of snow at the radar site.

5.4 Entrainment Velocity (w_e)

The entrainment velocities in Table 5 are within a factor of 2 - 3 of calculations made by Penc (1995) for the LOWS data. In the Penc entrainment velocity calculations, a lake-scale average for each major snow event was obtained using a kinematic equation for growth of a convective boundary layer initially presented by Deardorff and Peterson (1980). This technique uses boundary layer height differences averaged across the lake to compute growth rates, from which entrainment is derived. Our calculations apply only to the North Rose radar site, but are within expected ranges.

Results of Entrainment Velocity (w_e) Calculations 12-13 Jan 90

	12 Jan 0200UTC	12 Jan 0300UTC	12 Jan 0500UTC	12 Jan 1500UTC	13 Jan 1700UTC	13 Jan 2000UTC
Z_t (m)	1072	1140	835	2248	1742	1678
$\Delta\theta_t$ (K/m)	.9219	.748	.9038	3.502	12.9427	6.2171
C_q^2 (g/kg)^2	.0001	.00003981	.00003981	.00000794	.0000316	.00001995
Δq (g/kg/m)	-.392	-.675	-.353	.132	-.559	.170
Γ (k/m)	.002764	.002939	.000750	.002730	.002283	.007604
w_e (cm/sec)	**.85**	**.12**	**2.06**	**3.12**	**3.07**	**3.02**

Table 5. Values of variables derived from radar and rawinsonde data from 12-13 January 1990 used in calculating entrainment velocities along with their units.

The entrainment velocities in Table 5 are within a factor of 2 - 3 of calculations made by Penc (1995) for the LOWS data. In the Penc entrainment velocity calculations, a lake-scale average for each major snow event was obtained using a kinematic equation for growth of a convective boundary layer initially presented by Deardorff and Peterson (1980). This technique uses boundary layer height differences averaged across the lake to compute growth rates, from which entrainment is derived. Our calculations apply only to the North Rose radar site, but are within expected ranges.

Table 6 shows calculated entrainment velocities for two multiple snow band events. Due to limited rawinsonde data for the 25-26 February and 28 February - 1 March 1990 multiple snow band events, entrainment velocities could only be calculated for two time periods. The 25 February at 0300 UTC w_e calculation result appears rather large

Results of Entrainment Velocity (w_e) Calculations
25 Feb 90 and 28 Feb 90

	25 Feb 0300 UTC	28 Feb 1700 UTC
Z_i (m)	2184	3108
$\Delta\theta_v$ (K/m)	2.3289	9.5635
C_q^2 (g/kg)^2	.0002512	.00000199
Δq (g/kg/m)	.078	-.087
Γ (k/m)	.002500	.006252
w_e (cm/sec)	**20.61**	**2.15**

Table 6. Values of variables derived from radar and rawinsonde data from 25 February and 28 February 1990 used in calculating entrainment velocities along with their units.

compared with the results from Table 5. However, a rough order of magnitude calculation derived from Fig. 19 between 0200 and 0300 UTC reveals the boundary layer grew approximately 400m, or the entrainment velocity averaged 11.2 cm/sec. Because of the consistency between w_e determined from two approaches, the instantaneous entrainment velocity result for 0300 UTC appears to be reasonable.

6. Conclusions

Consistent with previous findings by White et al. (1991) for Type II CTBLs and cloudless convective boundary layers, gradients of moisture are the primary contributor to the radar index of refraction within a Type I CTBL, and therefore can be reliably sensed using vertical beam radars. The increased temporal resolution of the radar moisture analysis makes this an excellent tool for monitoring cloud-topped boundary layer depths. Moisture profiles obtained from satellites are sufficient for sensing the upper and mid-levels of the atmosphere.

However, because of the poor resolution of satellite-based moisture sensors for boundary layer application, wind profiler networks will remain necessary. Boundary layer height and cold front/trough passage can be gauged using the humidity data from these wind profiler radars. Additionally, using the assumption ($\alpha_r^2 = 1$) for a Type I CTBL is valid and will introduce very little error ($< 4\%$) in radar applications and modeling studies. Entrainment velocity rates and boundary layer growth can be reliably estimated using humidity-derived SNR radar data, as entrainment velocity calculations for the North Rose site were consistent with a lake-averaged kinematic equation for growth of the convective boundary layer. Also, rough order of magnitude entrainment velocity rates obtained from time-averaged radar data appeared to validate the instantaneous w_e calculations.

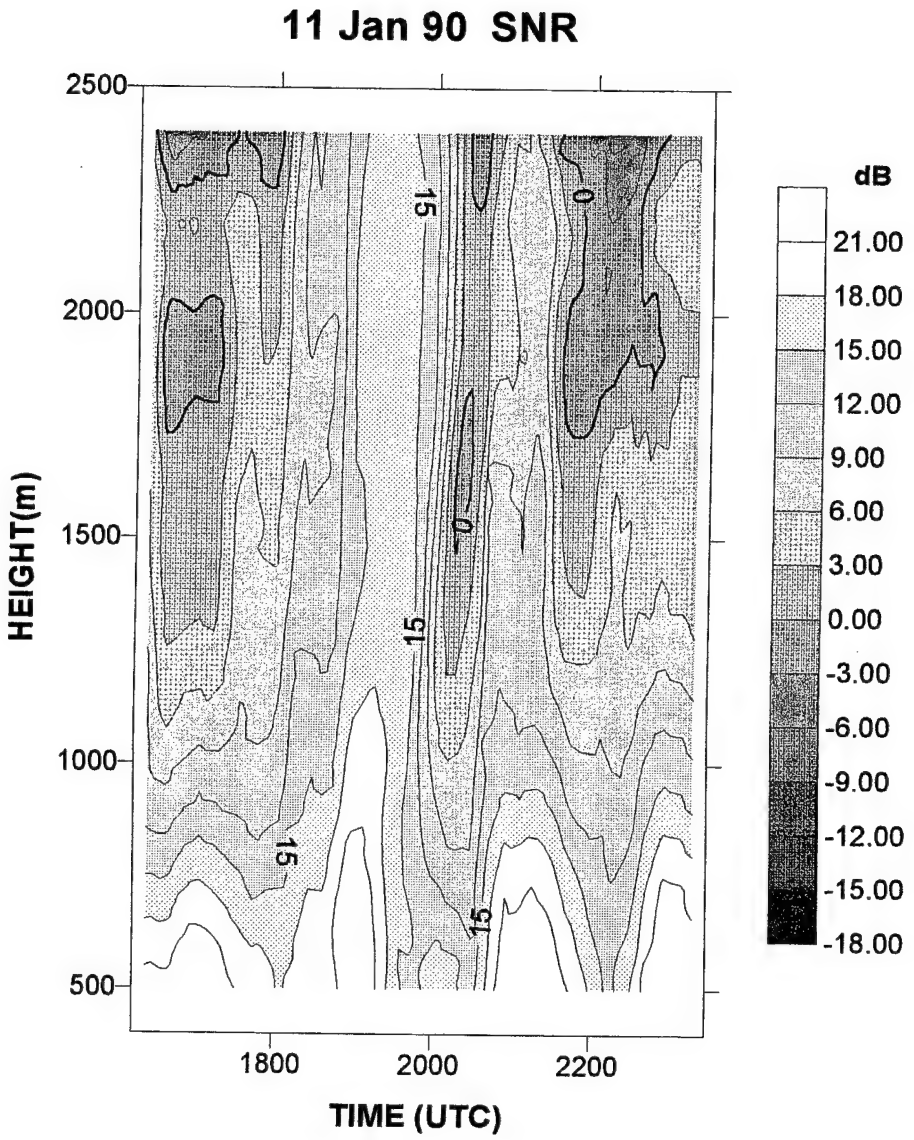
11 Jan 90 SNR
2500
2000
1500
1000
500
HEIGHT(m)
1800
2000
2200
TIME (UTC)
dB
21.00
18.00
15.00
12.00
9.00
6.00
3.00
0.00
-3.00
-6.00
-9.00
-12.00
-15.00
-18.00
15
0
-0
15
15
15

Fig 1

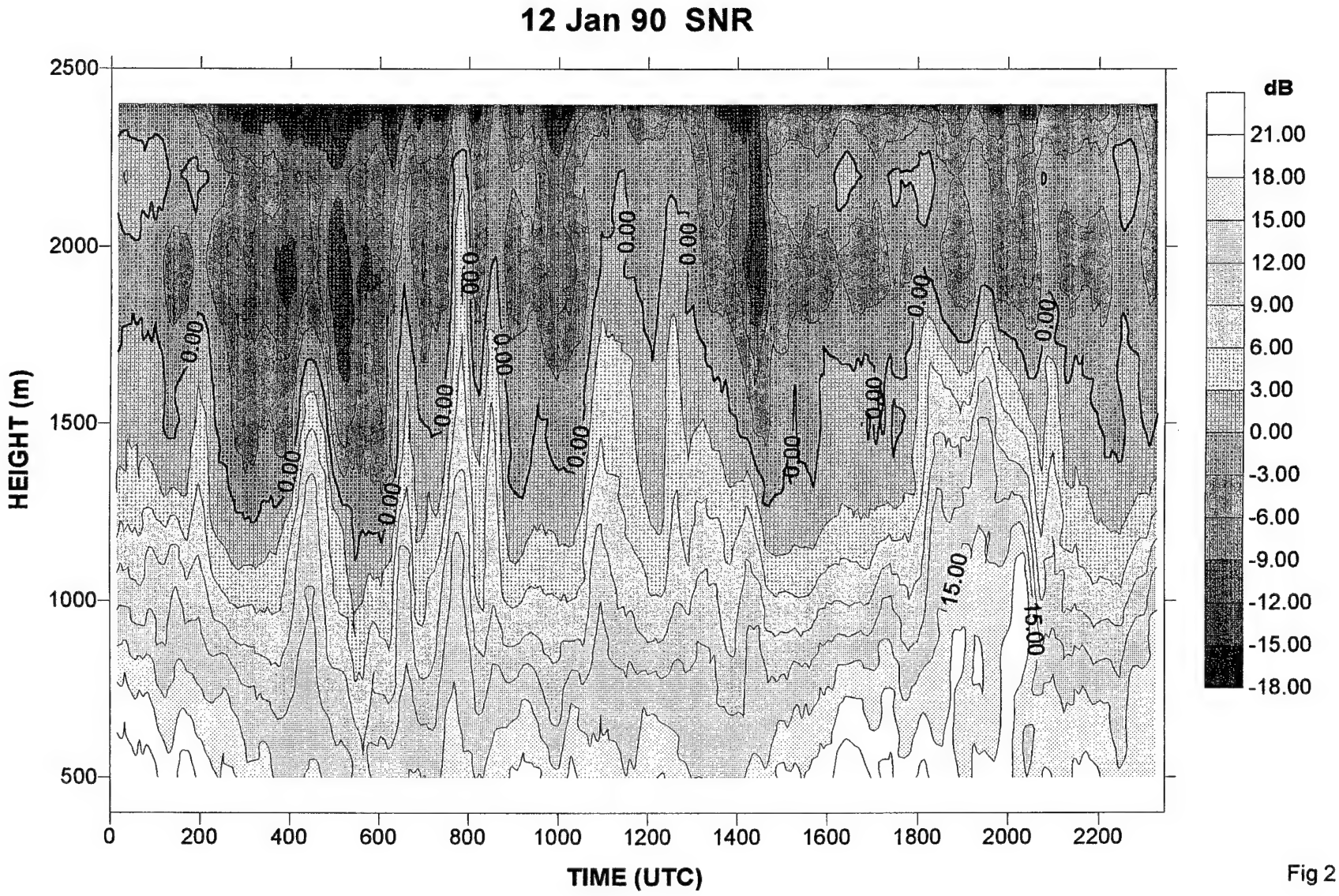
12 Jan 90 SNR
HEIGHT (m)
2500
2000
1500
1000
500
0
200
400
600
800
1000
1200
1400
1600
1800
2000
2200
TIME (UTC)
dB
21.00
18.00
15.00
12.00
9.00
6.00
3.00
0.00
-3.00
-6.00
-9.00
-12.00
-15.00
-18.00
0.00
15.00

Fig 2

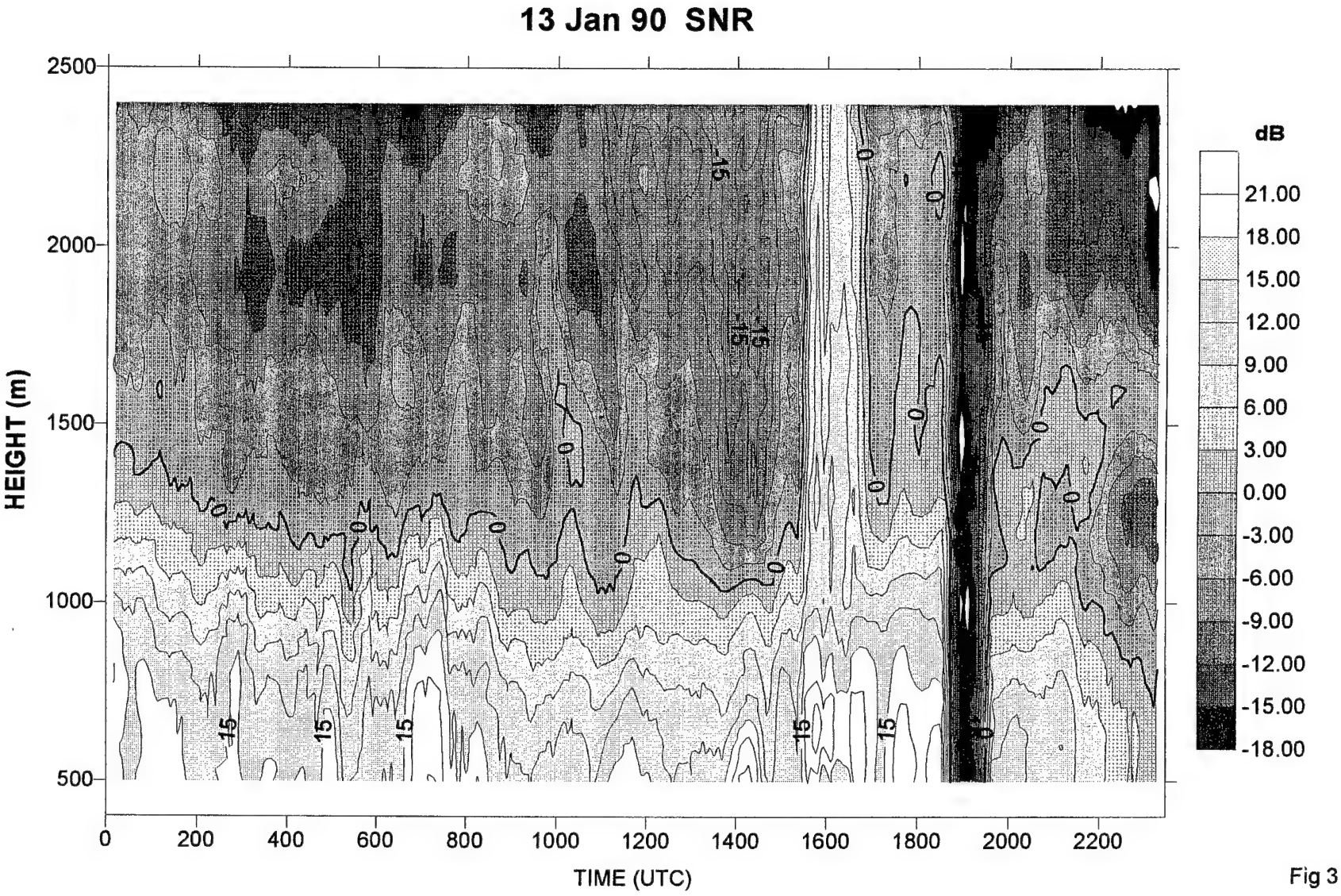
13 Jan 90 SNR
HEIGHT (m)
2500
2000
1500
1000
500
0
200
400
600
800
1000
1200
1400
1600
1800
2000
2200
TIME (UTC)
dB
21.00
18.00
15.00
12.00
9.00
6.00
3.00
0.00
-3.00
-6.00
-9.00
-12.00
-15.00
-18.00

Fig 3

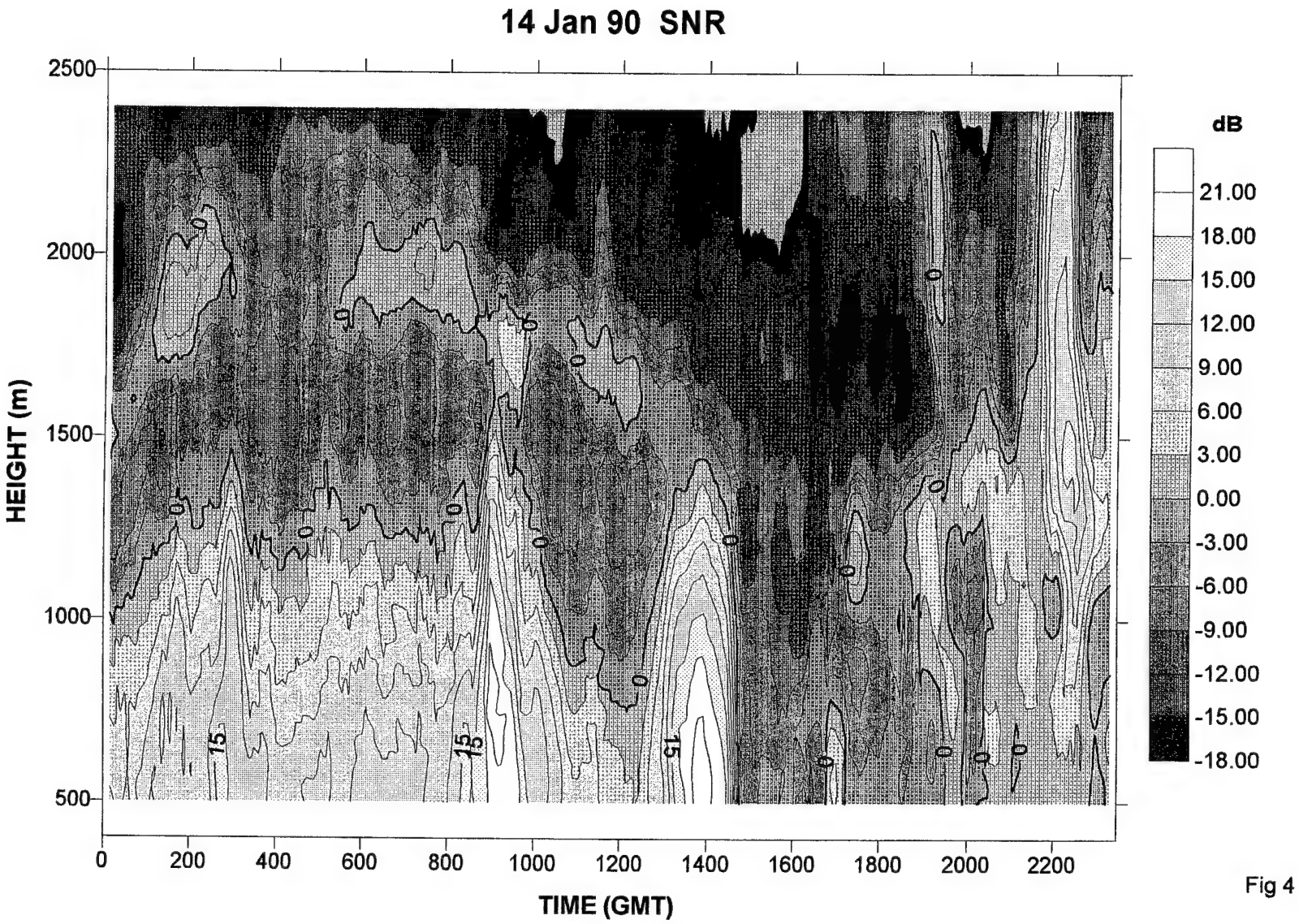
14 Jan 90 SNR
HEIGHT (m)
2500
2000
1500
1000
500
0
200
400
600
800
1000
1200
1400
1600
1800
2000
2200
TIME (GMT)
dB
21.00
18.00
15.00
12.00
9.00
6.00
3.00
0.00
-3.00
-6.00
-9.00
-12.00
-15.00
-18.00

Fig 4

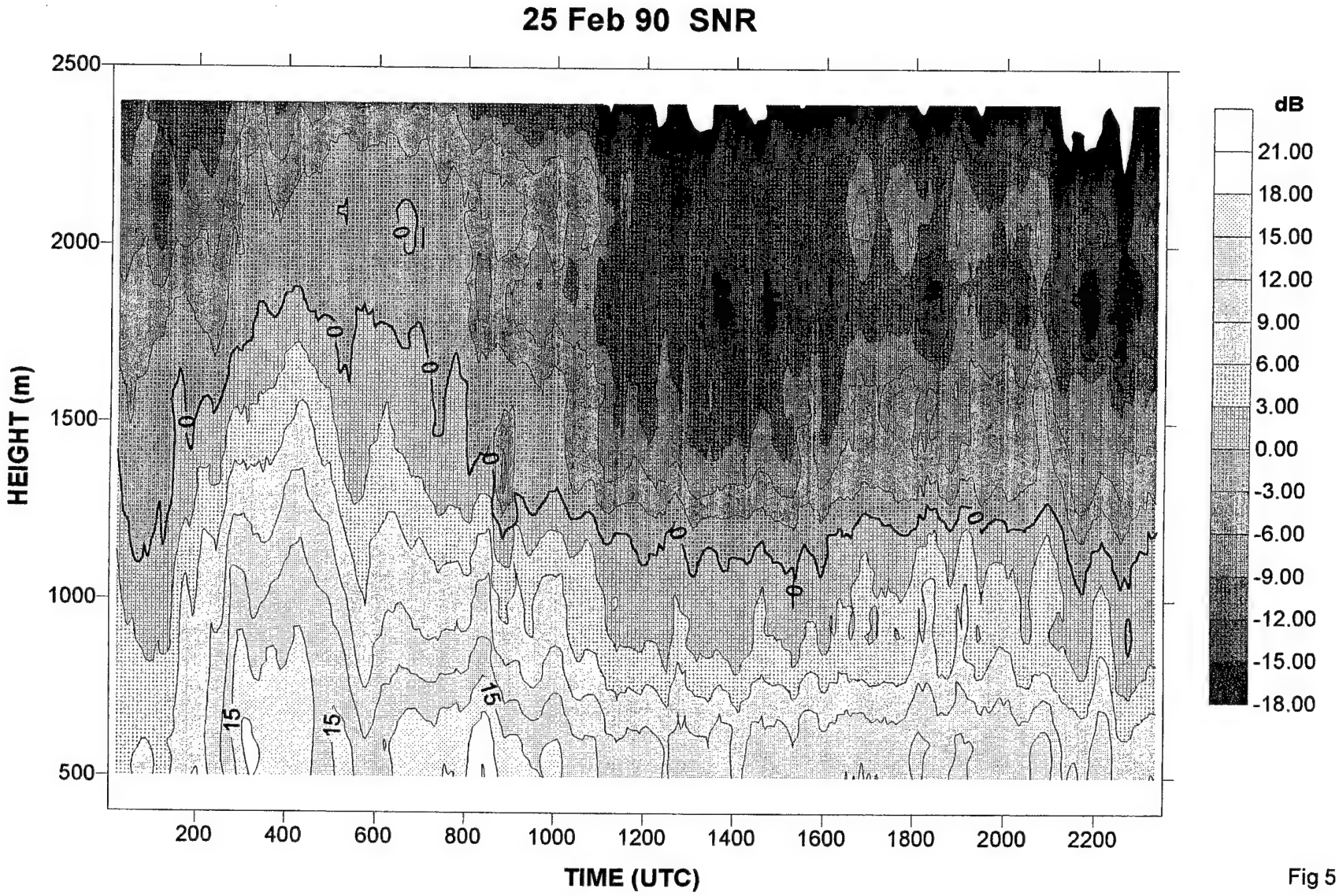
25 Feb 90 SNR
HEIGHT (m)
2500
2000
1500
1000
500
200
400
600
800
1000
1200
1400
1600
1800
2000
2200
TIME (UTC)
dB
21.00
18.00
15.00
12.00
9.00
6.00
3.00
0.00
-3.00
-6.00
-9.00
-12.00
-15.00
-18.00

Fig 5

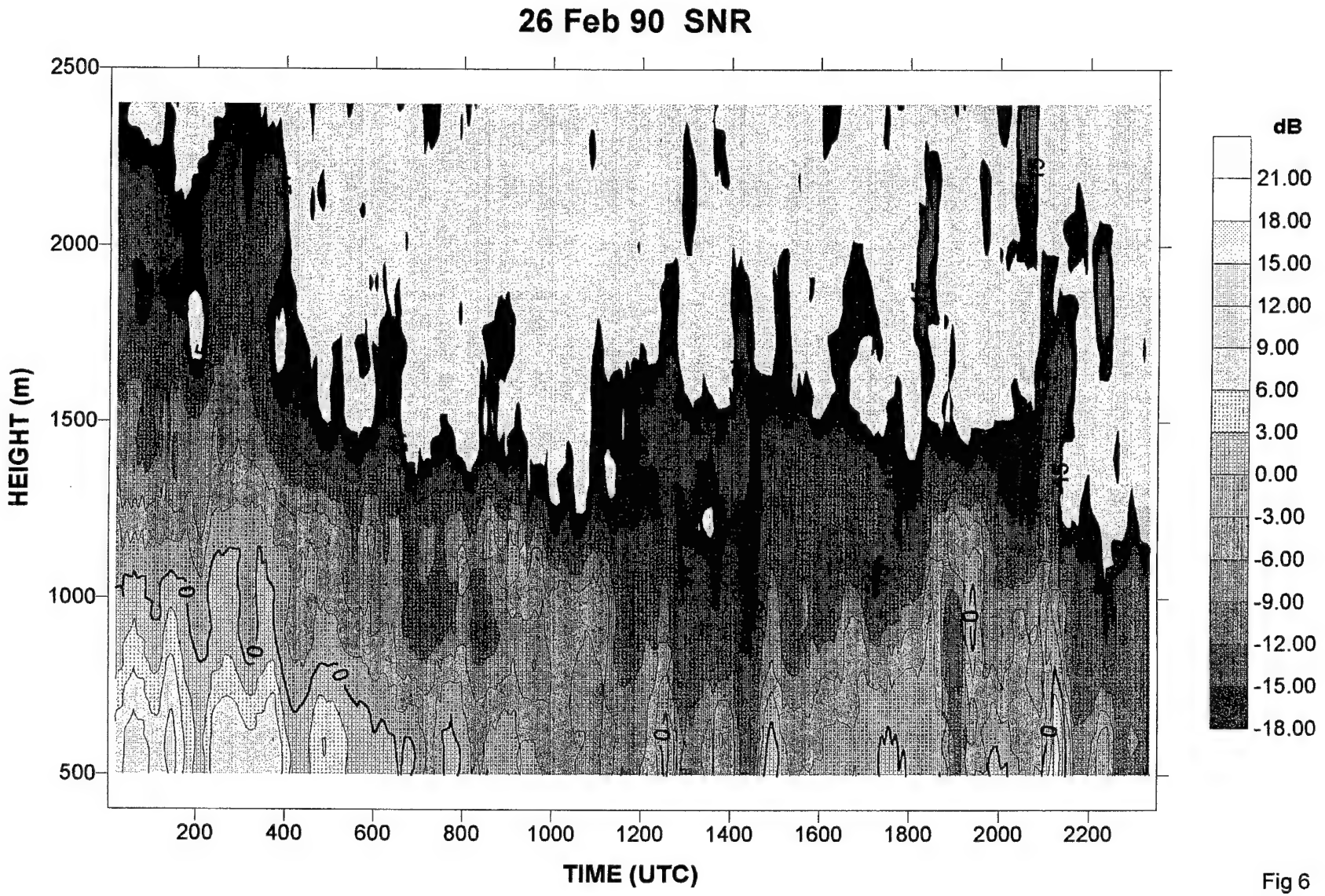
26 Feb 90 SNR
HEIGHT (m)
2500
2000
1500
1000
500
200
400
600
800
1000
1200
1400
1600
1800
2000
2200
TIME (UTC)
dB
21.00
18.00
15.00
12.00
9.00
6.00
3.00
0.00
-3.00
-6.00
-9.00
-12.00
-15.00
-18.00

Fig 6

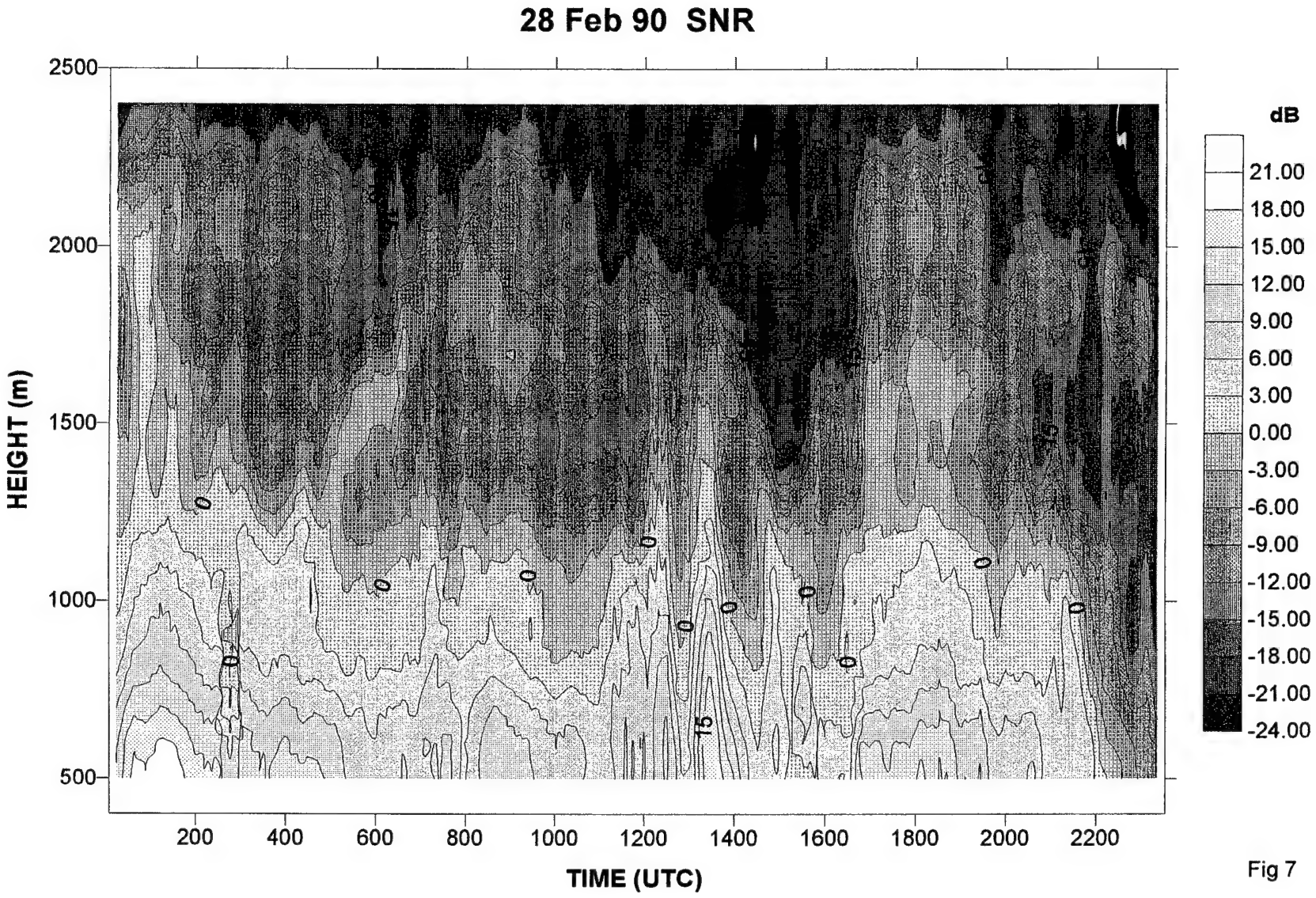
28 Feb 90 SNR
HEIGHT (m)
2500
2000
1500
1000
500
200
400
600
800
1000
1200
1400
1600
1800
2000
2200
TIME (UTC)
dB
21.00
18.00
15.00
12.00
9.00
6.00
3.00
0.00
-3.00
-6.00
-9.00
-12.00
-15.00
-18.00
-21.00
-24.00

Fig 7

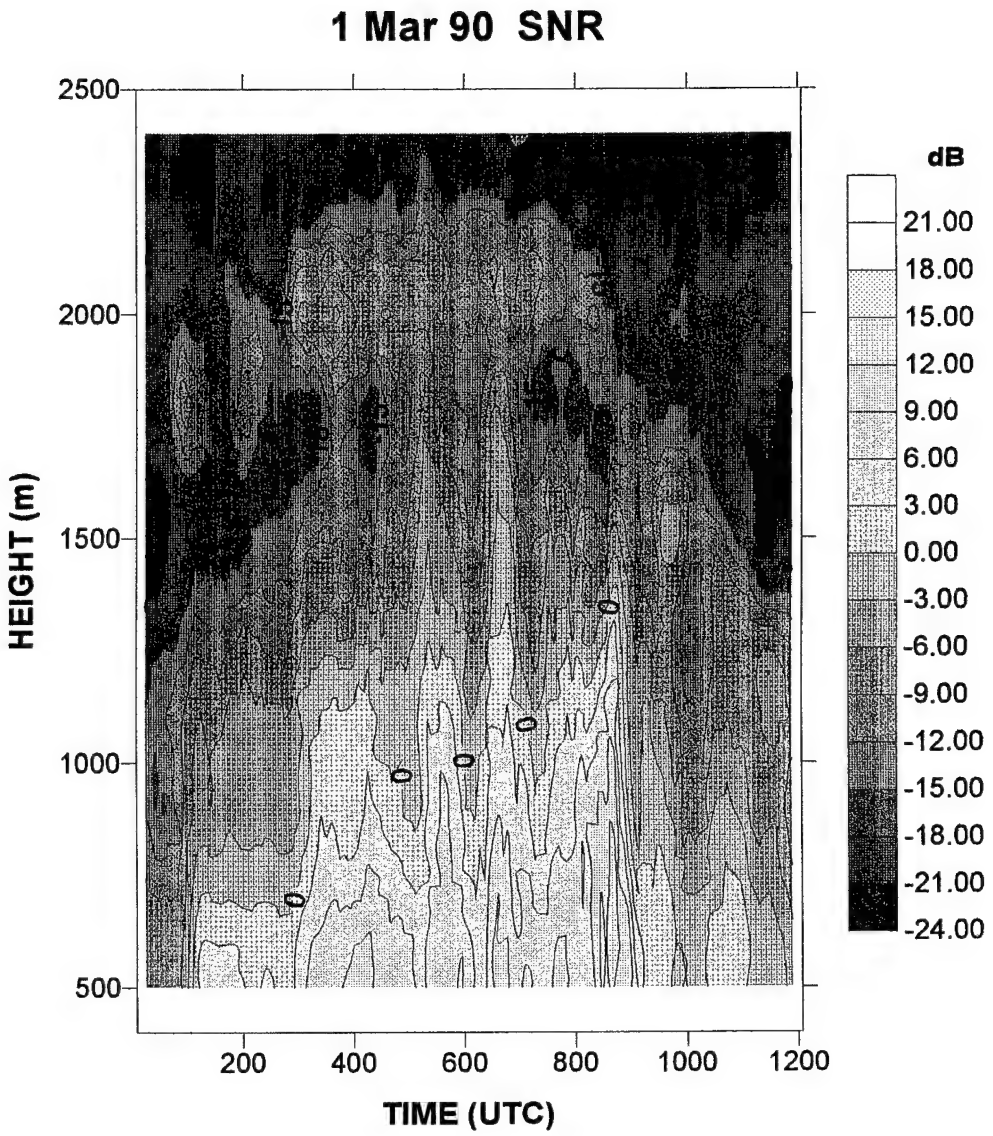
1 Mar 90 SNR
2500
2000
1500
1000
500
HEIGHT (m)
200
400
600
800
1000
1200
TIME (UTC)
dB
21.00
18.00
15.00
12.00
9.00
6.00
3.00
0.00
-3.00
-6.00
-9.00
-12.00
-15.00
-18.00
-21.00
-24.00

Fig 8

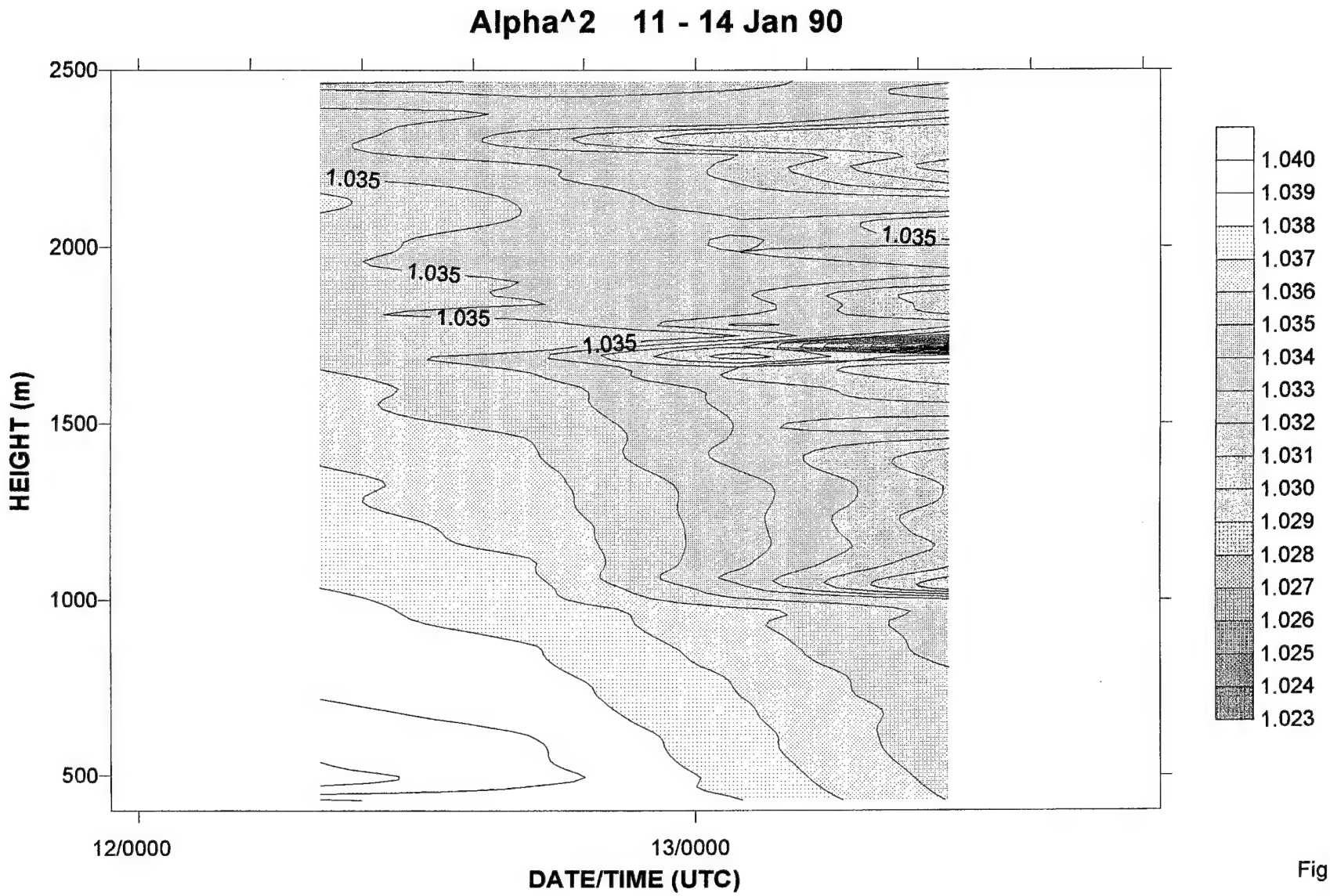
Alpha^2 11 - 14 Jan 90
2500
2000
1500
1000
500
HEIGHT (m)
1.035
1.035
1.035
1.035
1.035
12/0000
13/0000
DATE/TIME (UTC)
1.040
1.039
1.038
1.037
1.036
1.035
1.034
1.033
1.032
1.031
1.030
1.029
1.028
1.027
1.026
1.025
1.024
1.023

Fig 9

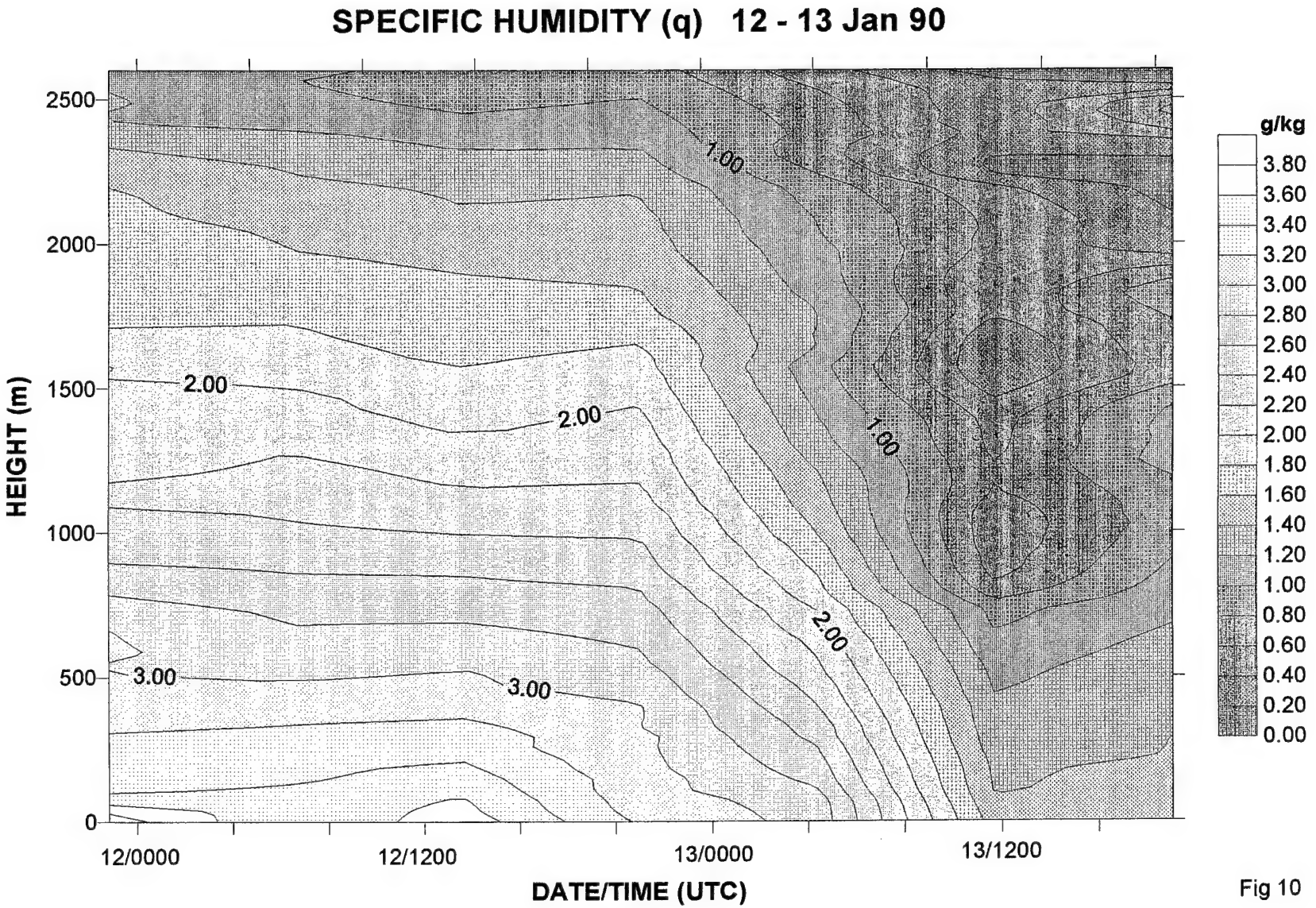
SPECIFIC HUMIDITY (q) 12 - 13 Jan 90
HEIGHT (m)
2500
2000
1500
1000
500
0
1.00
2.00
2.00
1.00
2.00
3.00
3.00
12/0000
12/1200
13/0000
13/1200
DATE/TIME (UTC)
g/kg
3.80
3.60
3.40
3.20
3.00
2.80
2.60
2.40
2.20
2.00
1.80
1.60
1.40
1.20
1.00
0.80
0.60
0.40
0.20
0.00

Fig 10

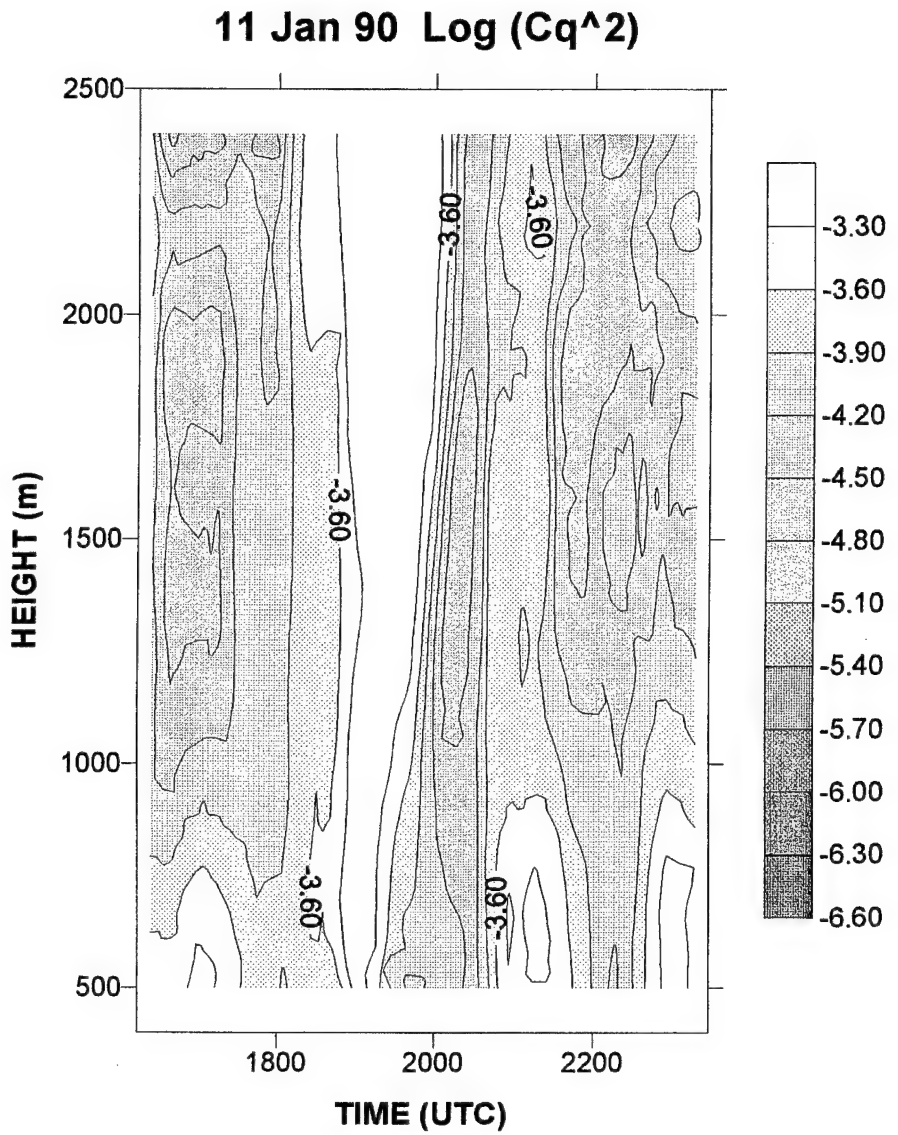
11 Jan 90 Log (Cq^2)
2500
2000
1500
1000
500
HEIGHT (m)
-3.60
-3.60
-3.60
-3.60
1800
2000
2200
TIME (UTC)
-3.30
-3.60
-3.90
-4.20
-4.50
-4.80
-5.10
-5.40
-5.70
-6.00
-6.30
-6.60

Fig 11

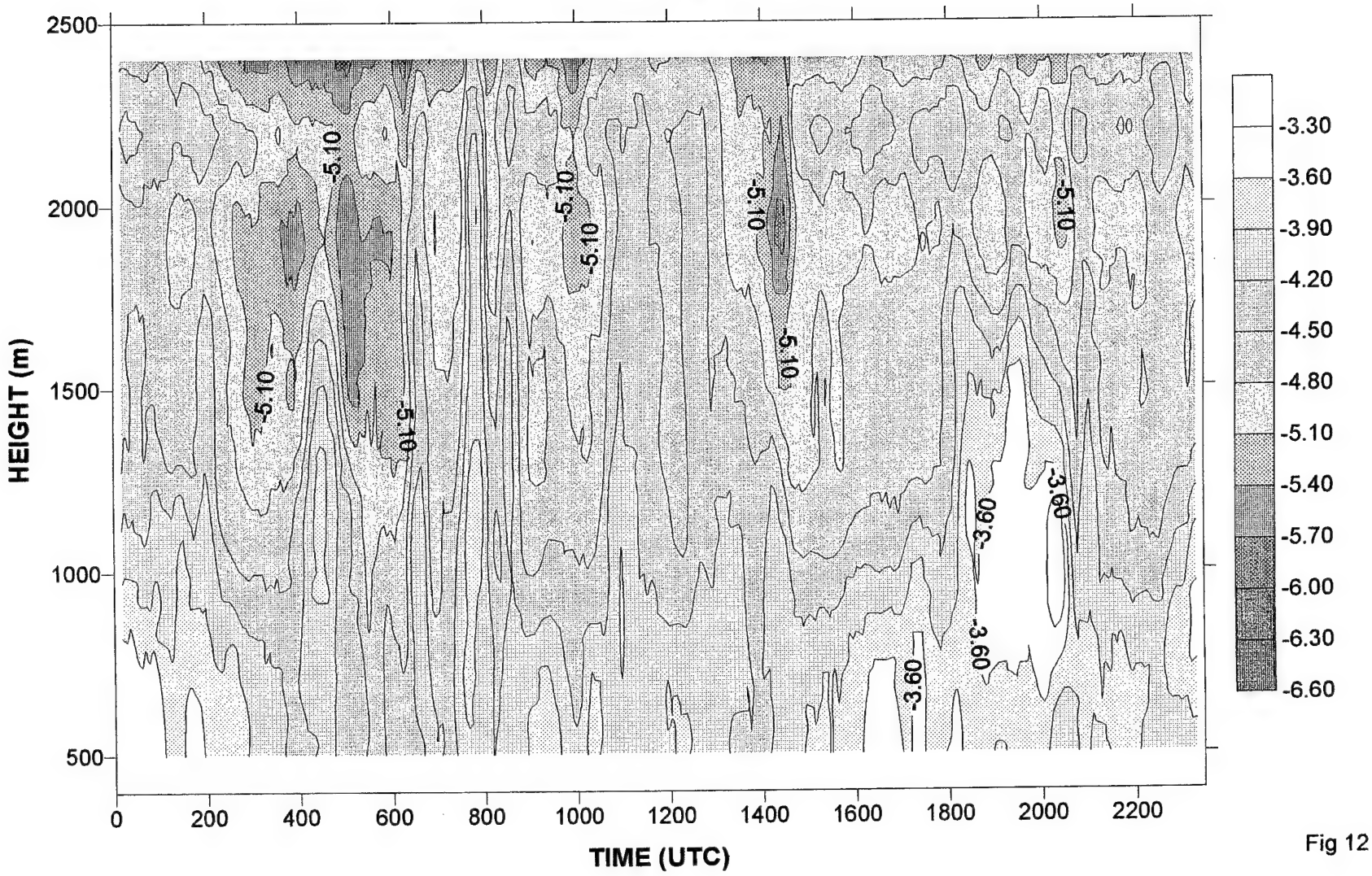
12 Jan 90 Log (Cq^2)
HEIGHT (m)
2500
2000
1500
1000
500
0
200
400
600
800
1000
1200
1400
1600
1800
2000
2200
TIME (UTC)
-5.10
-3.60
-3.30
-3.60
-3.90
-4.20
-4.50
-4.80
-5.10
-5.40
-5.70
-6.00
-6.30
-6.60

Fig 12

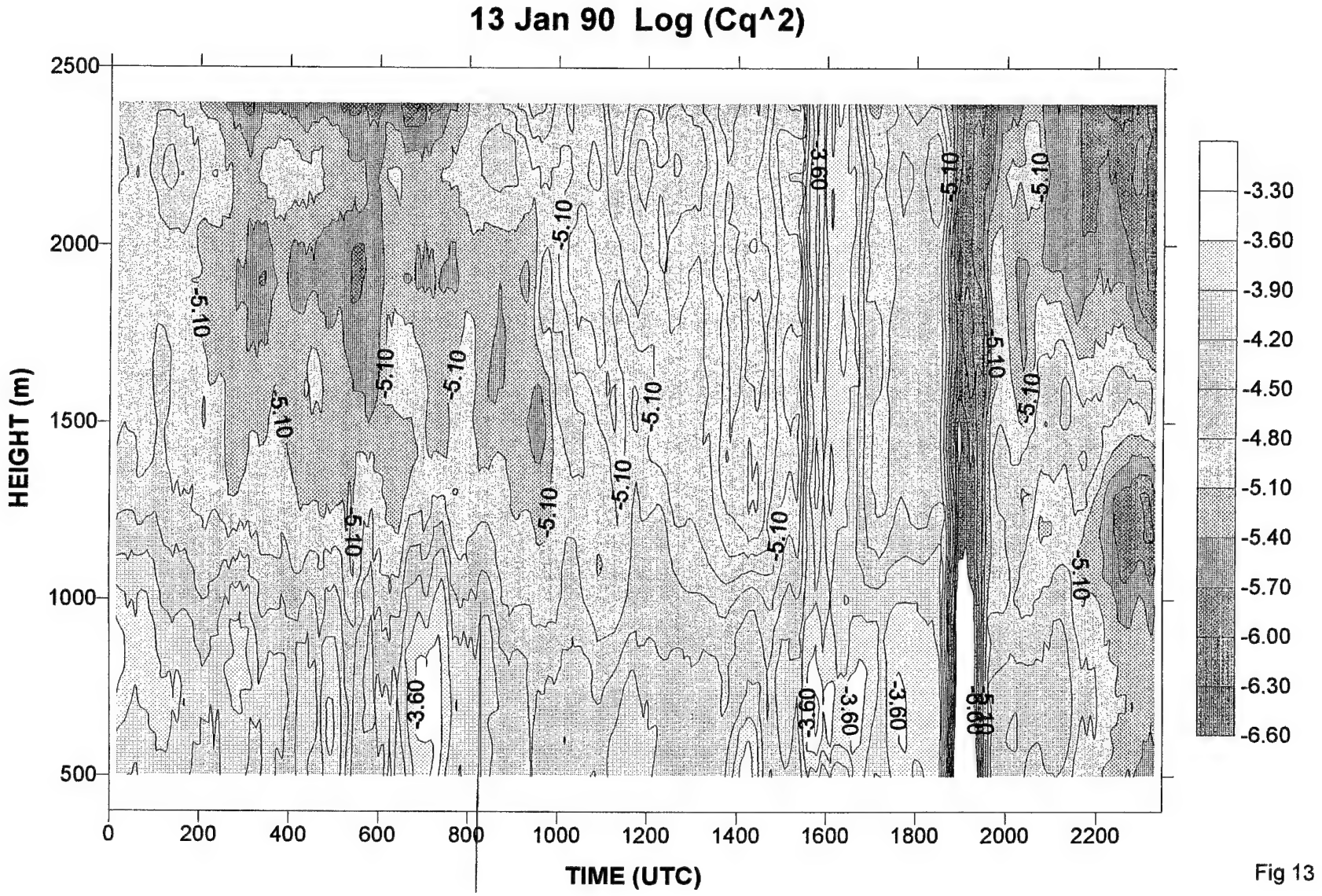
13 Jan 90 Log (Cq^2)
HEIGHT (m)
2500
2000
1500
1000
500
0
200
400
600
800
1000
1200
1400
1600
1800
2000
2200
TIME (UTC)
-3.30
-3.60
-3.90
-4.20
-4.50
-4.80
-5.10
-5.40
-5.70
-6.00
-6.30
-6.60

Fig 13

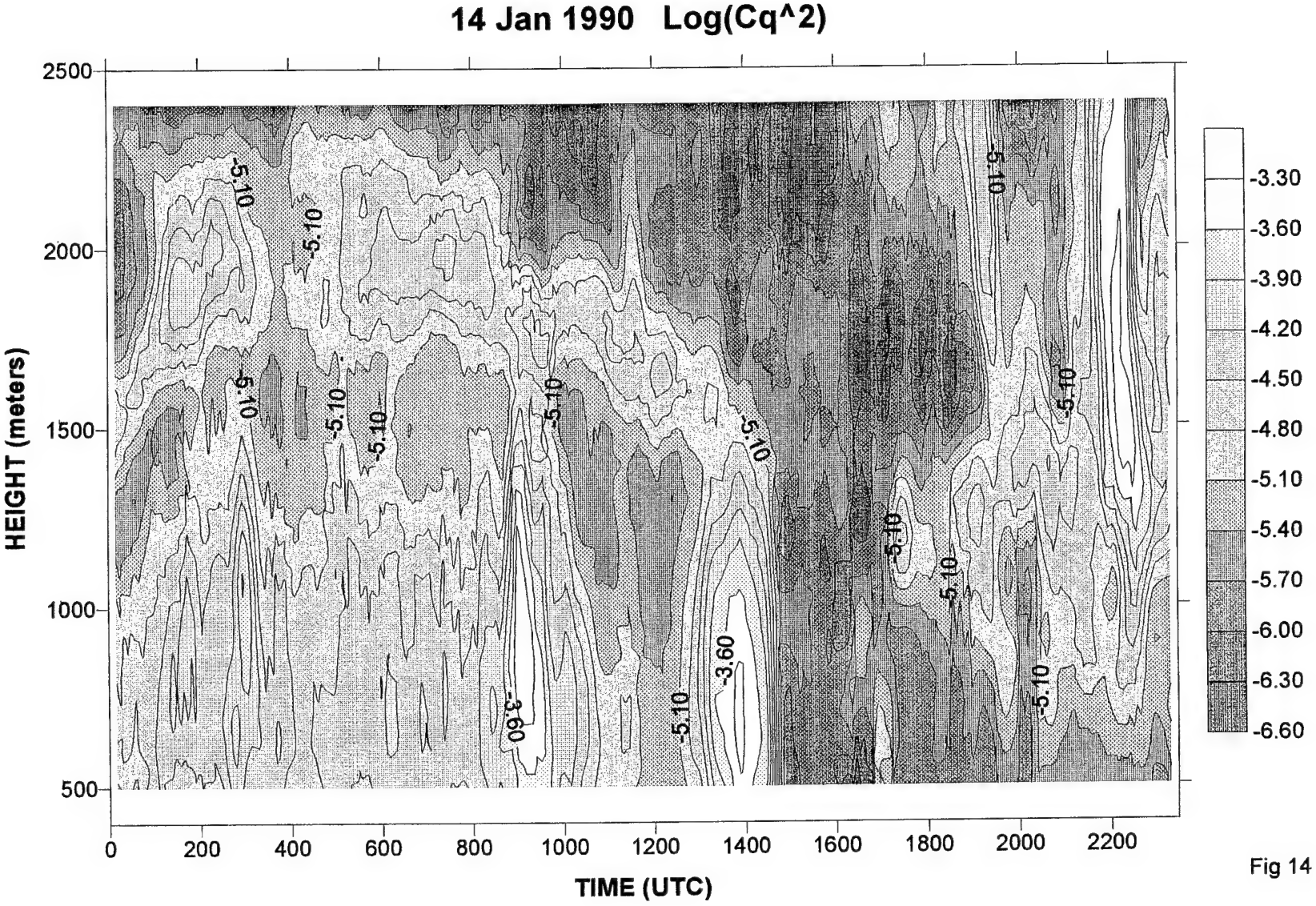
14 Jan 1990 Log(Cq^2)
HEIGHT (meters)
2500
2000
1500
1000
500
0
200
400
600
800
1000
1200
1400
1600
1800
2000
2200
TIME (UTC)
-3.30
-3.60
-3.90
-4.20
-4.50
-4.80
-5.10
-5.40
-5.70
-6.00
-6.30
-6.60

Fig 14

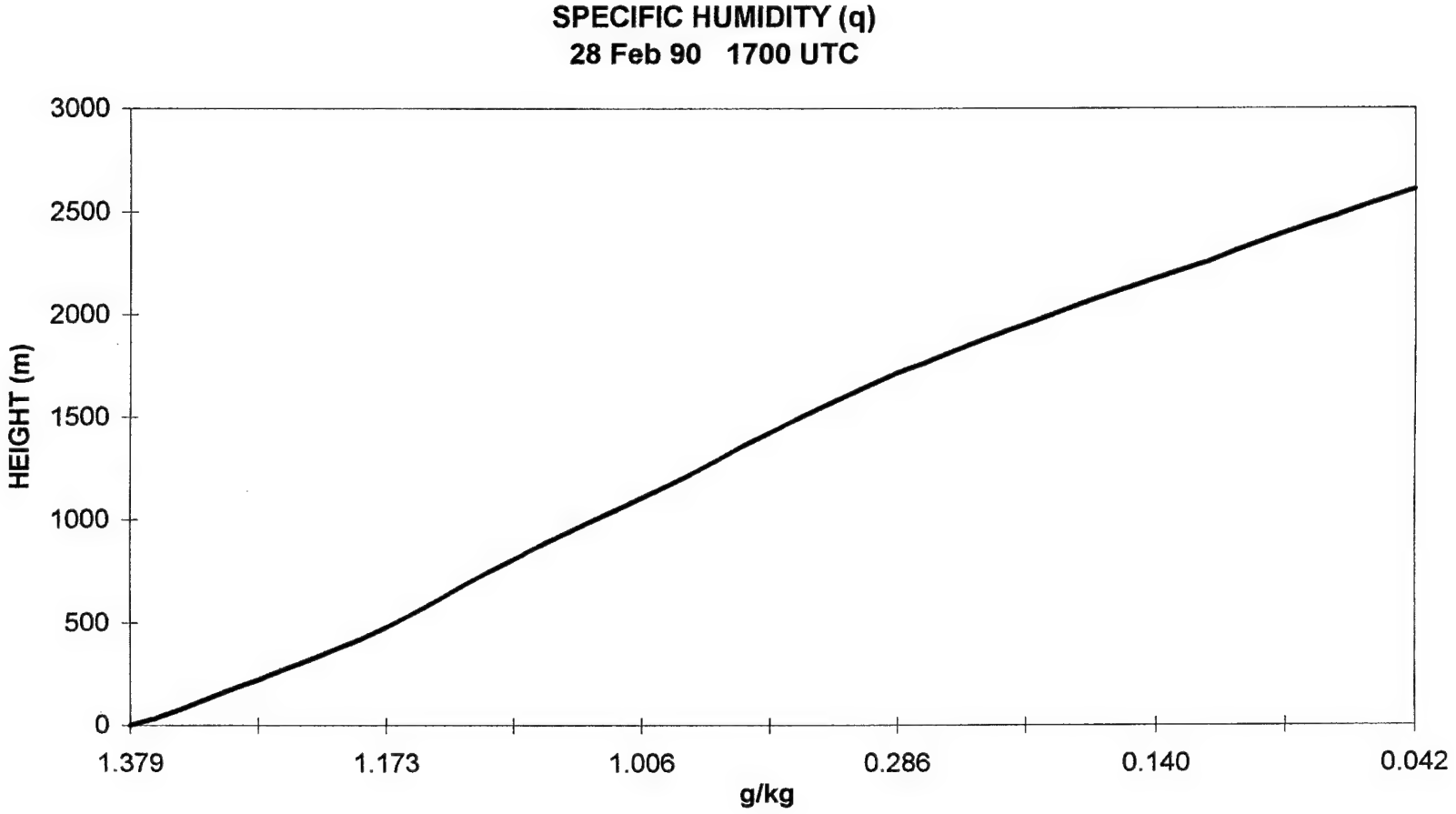
SPECIFIC HUMIDITY (q)
28 Feb 90 1700 UTC
HEIGHT (m)
3000
2500
2000
1500
1000
500
0
1.379
1.173
1.006
0.286
0.140
0.042
g/kg

Fig 15

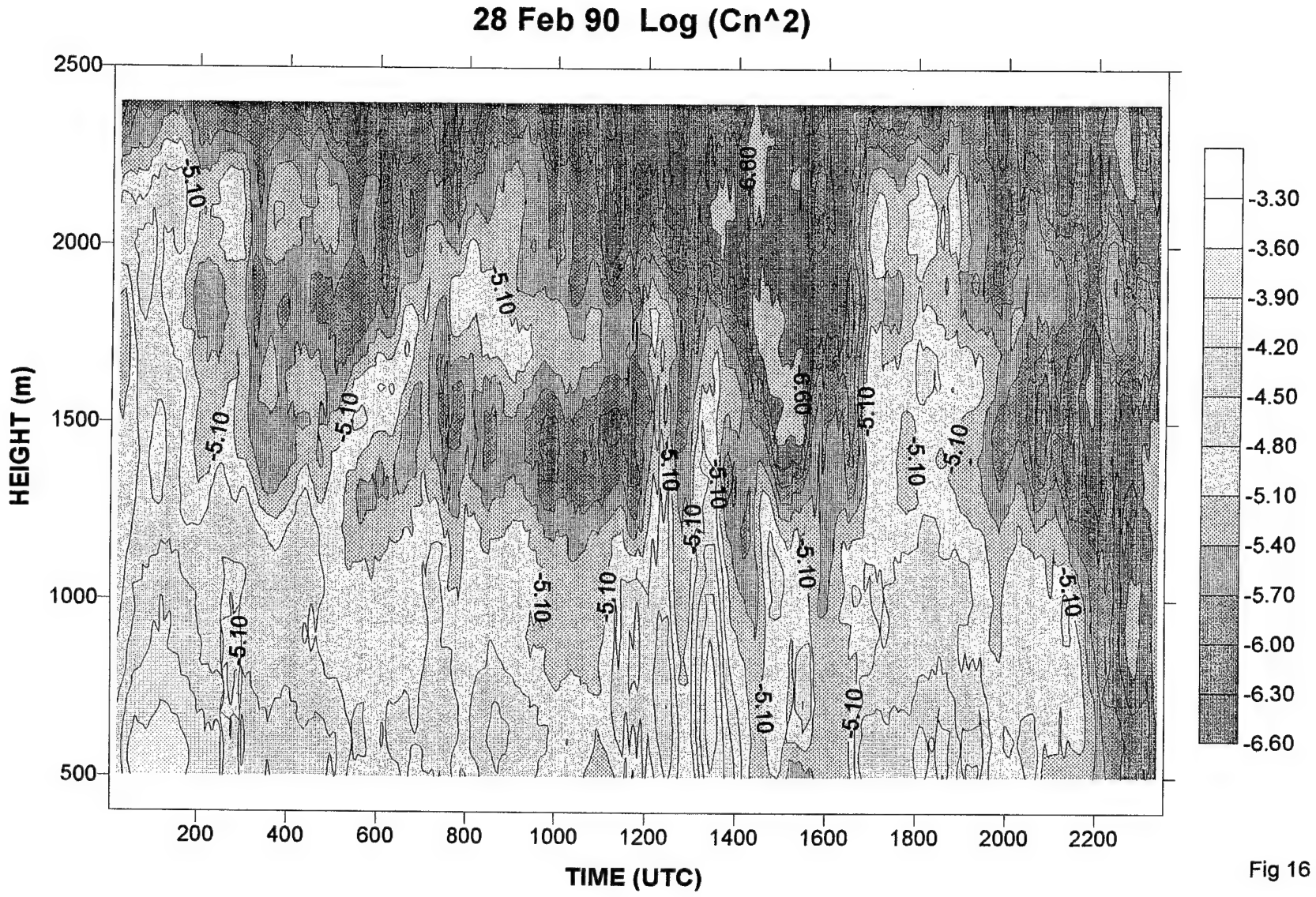
28 Feb 90 Log (Cn^2)
HEIGHT (m)
2500
2000
1500
1000
500
200
400
600
800
1000
1200
1400
1600
1800
2000
2200
TIME (UTC)
-3.30
-3.60
-3.90
-4.20
-4.50
-4.80
-5.10
-5.40
-5.70
-6.00
-6.30
-6.60

Fig 16

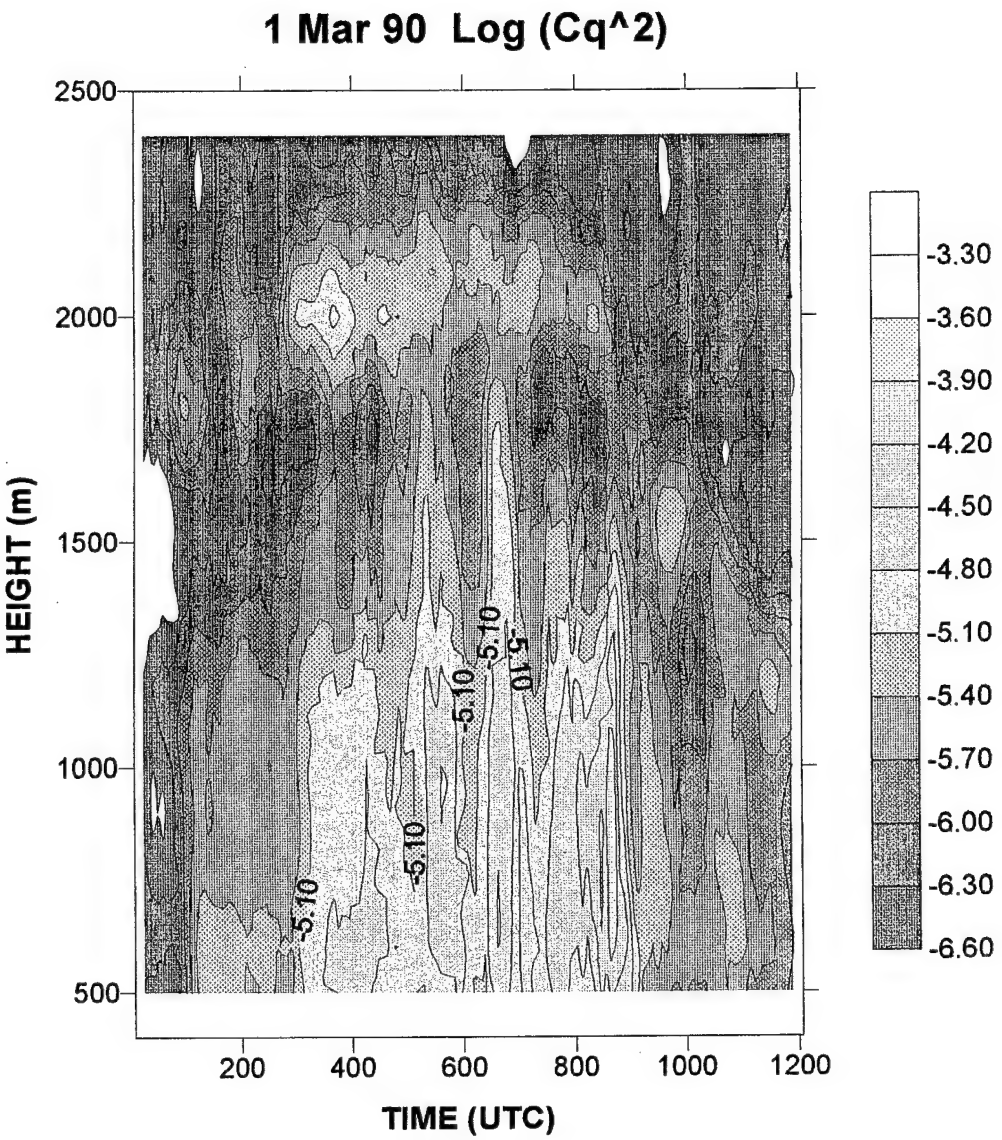
1 Mar 90 Log (Cq^2)
2500
2000
1500
1000
500
HEIGHT (m)
200
400
600
800
1000
1200
TIME (UTC)
-5.10
-5.10
-5.10
-5.10
-5.10
-3.30
-3.60
-3.90
-4.20
-4.50
-4.80
-5.10
-5.40
-5.70
-6.00
-6.30
-6.60

Fig 17

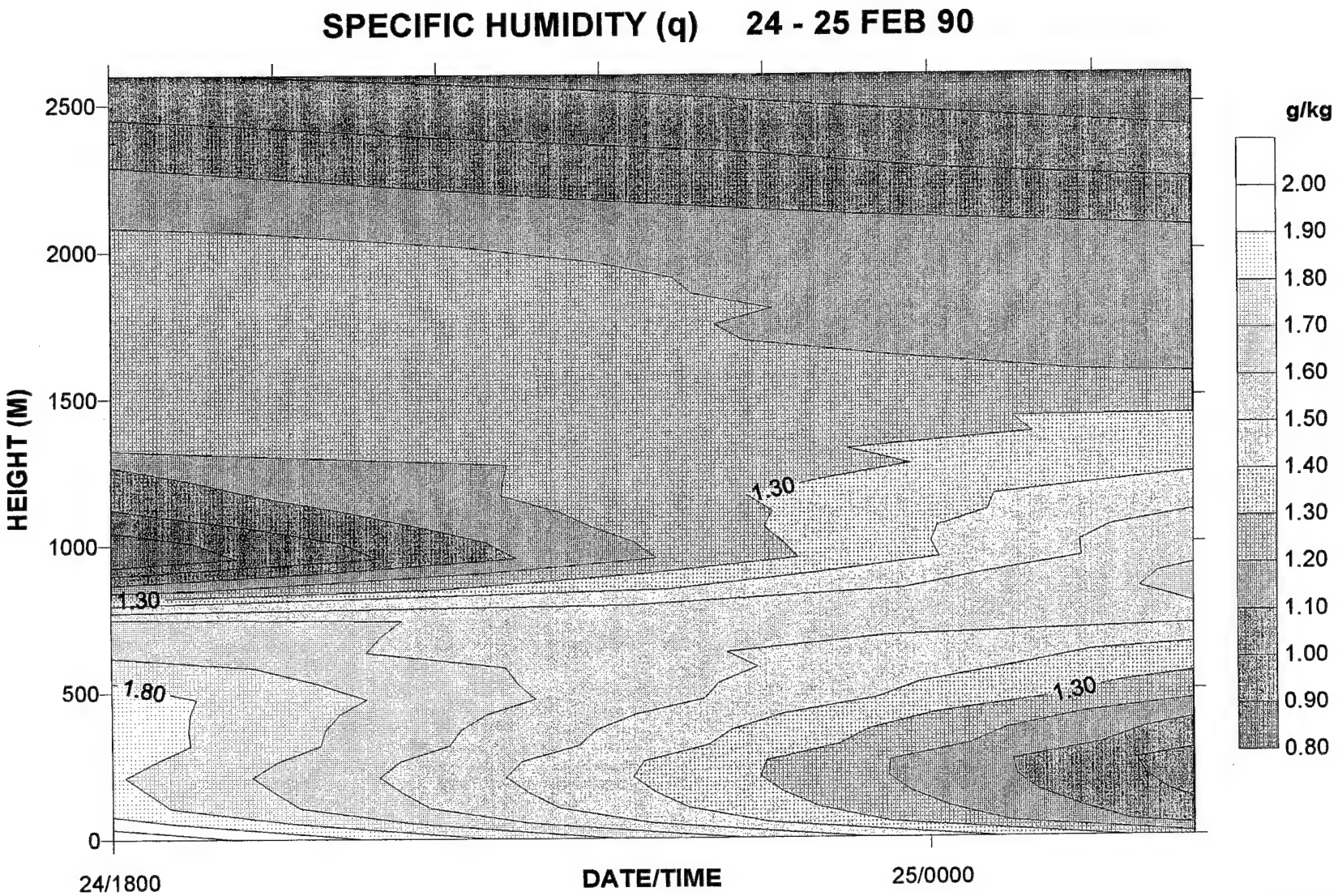
SPECIFIC HUMIDITY (q) 24 - 25 FEB 90
HEIGHT (M)
2500
2000
1500
1000
500
0
1.30
1.80
1.30
1.30
DATE/TIME
24/1800
25/0000
g/kg
2.00
1.90
1.80
1.70
1.60
1.50
1.40
1.30
1.20
1.10
1.00
0.90
0.80

Fig 18

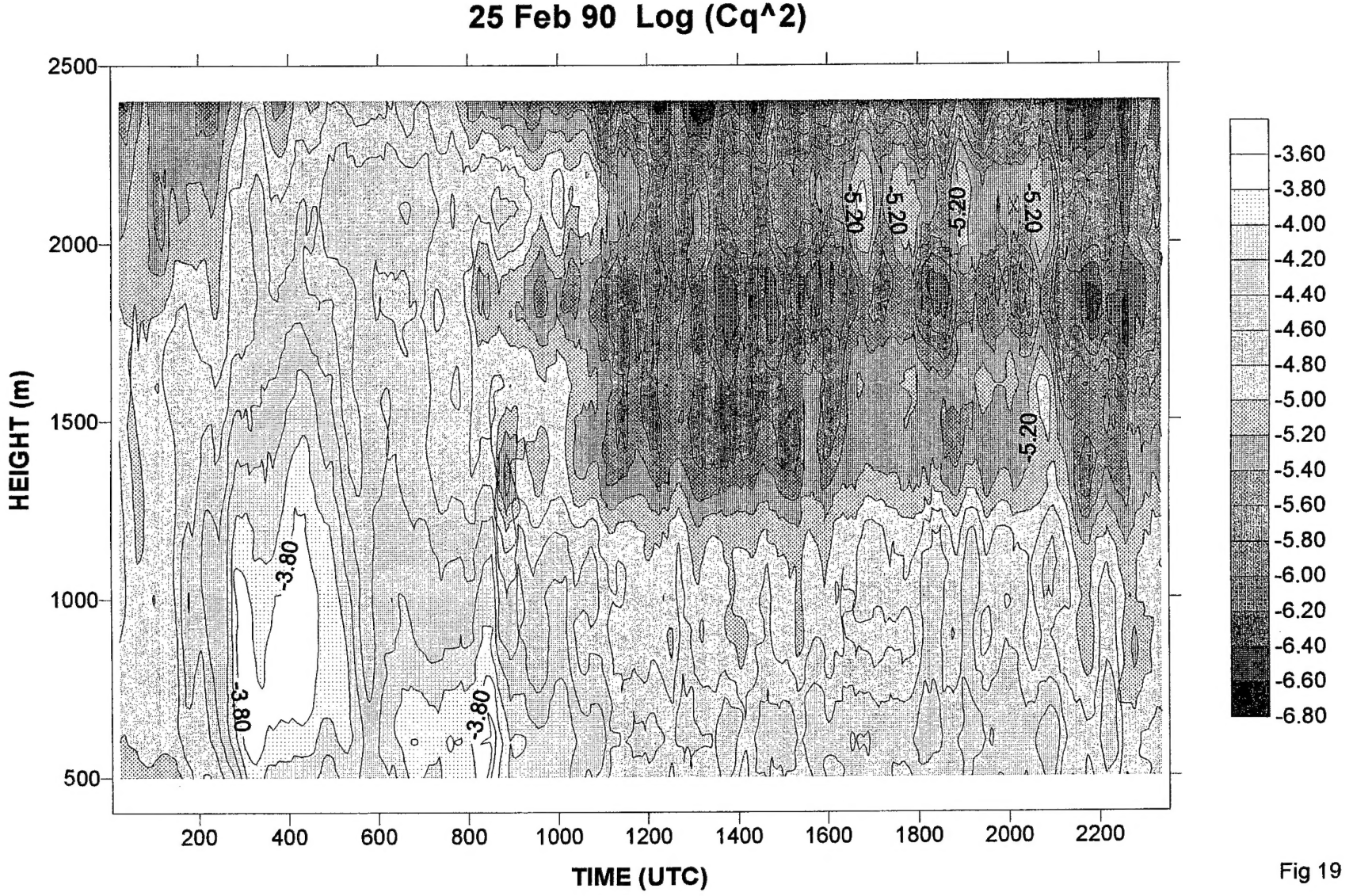
25 Feb 90 Log (Cq^2)
HEIGHT (m)
2500
2000
1500
1000
500
200
400
600
800
1000
1200
1400
1600
1800
2000
2200
TIME (UTC)
-3.80
-3.80
-3.80
-5.20
-5.20
-5.20
-5.20
-5.20
-3.60
-3.80
-4.00
-4.20
-4.40
-4.60
-4.80
-5.00
-5.20
-5.40
-5.60
-5.80
-6.00
-6.20
-6.40
-6.60
-6.80

Fig 19

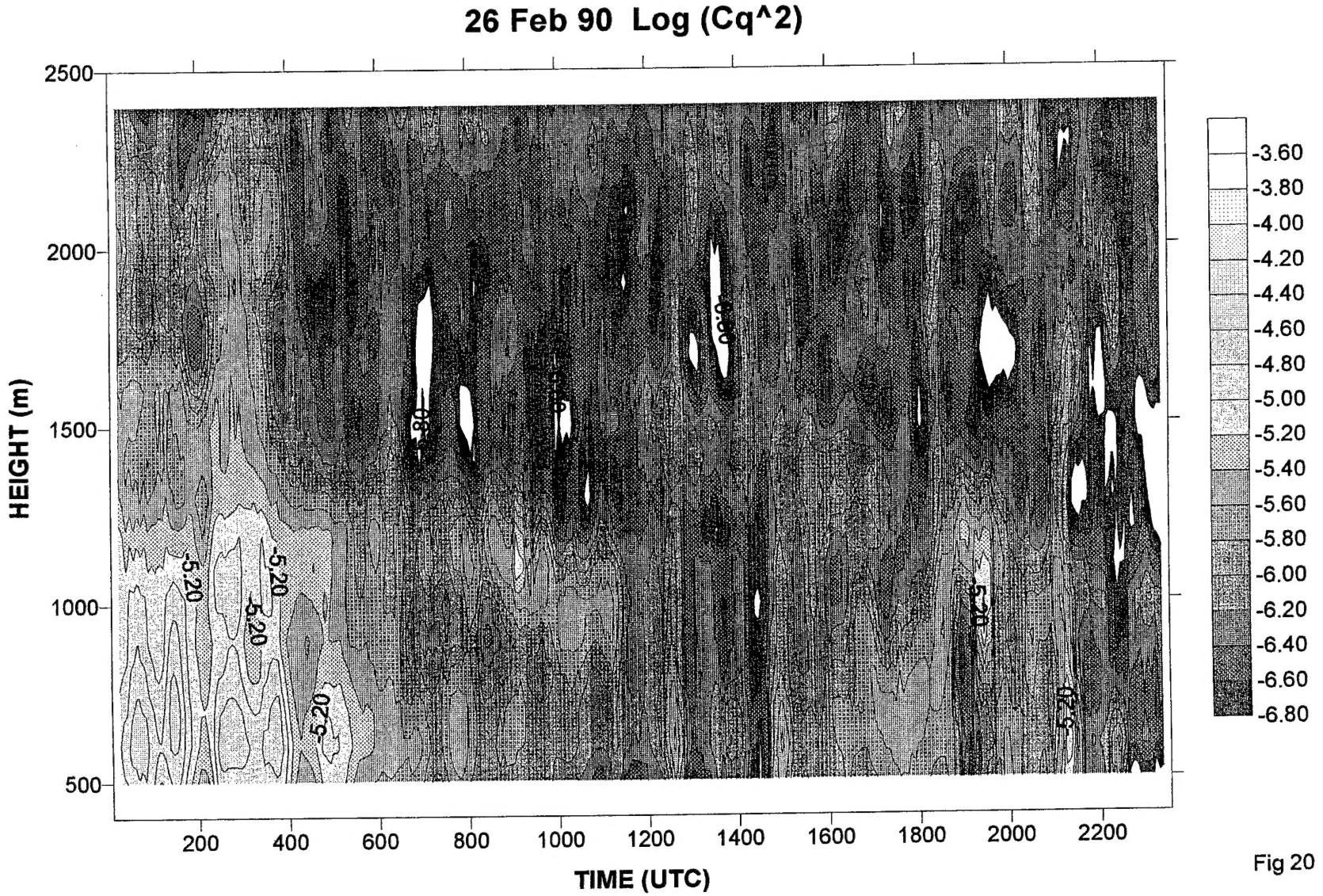
26 Feb 90 Log (Cq^2)
HEIGHT (m)
2500
2000
1500
1000
500
200
400
600
800
1000
1200
1400
1600
1800
2000
2200
TIME (UTC)
-3.60
-3.80
-4.00
-4.20
-4.40
-4.60
-4.80
-5.00
-5.20
-5.40
-5.60
-5.80
-6.00
-6.20
-6.40
-6.60
-6.80

Fig 20

References

Agee, E.M., and M.L. Hart, 1990: Boundary Layer and Mesoscale Structure over Lake Michigan during a Wintertime Cold Air Outbreak. *Journal of Atmospheric Sciences*, **47**, 2293-2316.

Burk, S.D., 1981: Temperature and Humidity Effects on Refractive Index Fluctuations in Upper Regions of the Convective Boundary Layer. *Journal of Applied Meteorology*, **20**, 717-721.

Cohn, S.A., 1995: Radar Measurements of Turbulent Eddy Dissipation Rate in the Troposphere: A Comparison of Techniques. *Journal of Atmospheric and Oceanic Technology*, **12**, 85-95.

Fairall, W.C., 1991: The Humidity and Temperature Sensitivity of Clear Air Radars in the Convective Boundary Layer. *Journal of Applied Meteorology*, **30**, 1064-1074.

Gossard, E.E., and R.G. Strauch, 1983: *Radar Observations of Clear Air and Clouds*, Elsevier, 280pp.

Lavoie, R.L., 1972: A Mesoscale Numerical Model of Lake Effect Storms. *Journal of Atmospheric Sciences*, **29**, 1025-1040.

Niziol, T.A., 1987: Operational Forecasting of Lake Effect Snowfall in Western and Central New York. *Weather Forecasting*, **2**, 310-321.

Ottersten, H., 1969: Atmosphere Structure and Radar Backscattering in Clear Air. *Radio Science*, **4**, 1179-1193.

Peace, R.L., Jr., and R.B. Sykes, Jr., 1966: Mesoscale Study of a Lake Effect Snow Storm. *Monthly Weather Review*, **94**, 495-507.

Penc, R.S., 1991: Observations of Lake Effect Snowstorms using a RASS-equipped UHF Wind Profiler. *Second Symposium on Tropospheric Profiling: needs and technologies*. Boulder, Colorado, 10-13 September 1991.

Penc, R.S., 1991: Performance of a RASS-equipped UHF Wind Profiler in the Environment of Lake-Effect Storms. *Second Symposium on Tropospheric Profiling: needs and technologies*. Boulder, Colorado, 10-13 September 1991.

Penc, R.S., Dec. 1995: Observations of the Mesoscale Environment and Convective Mixed Layer Developing During Lake-Effect Snow Situations, Ph.D. Thesis, The Pennsylvania State University, Department of Meteorology, University Park, PA., 164pp.

Reinking, R.F., R. Caiazza, R.A. Kropfli, B.W. Orr, B.E. Martner, T.A. Niziol, G.P. Byrd, R.S. Penc, R.J. Zamora, J.B. Snider, R.J. Ballentine, A.J. Stamm, C.D. Bedford, P. Joe, and A.J. Koscielny, 1993: The Lake Ontario Winter Storms (LOWS) Project. *Bulletin of the American Meteorological Society*, **74**, 1828-1849.

Strauch, R.G., D.A. Merrit, K.P. Moran, K.B. Earnshaw, and D. Van de Kamp, 1984: The Colorado wind-profiling network. *Journal of Atmospheric and Oceanic Technology*, **1**, 37-49. et al (1984)

Stull, R.B., 1988: *An Introduction to Boundary Layer Meteorology*, Kluwer Academic Publishers, 670pp.

Tatarski, V.I., 1961: *Wave Propagation in a Turbulent Medium*, McGraw Hill, 285pp.

VanZandt, T.E., J.L. Green, K.S. Gage, and W.L. Clark, 1978: Vertical Profiles of Refractive Turbulence Structure Constant: Comparison of Observations by the Sunset Radar with a new Theoretical Model. *Radio Science*, **13**, 5.

Wallace, J.M., and P.V. Hobbs, 1977: *Atmospheric Science: An Introduction Survey*, Academic Press, Inc., 467pp.

Wesley, M.L., 1976: The Combined Effect of Temperature and Humidity Fluctuations on Refractive Index. *Journal of Applied Meteorology*, **15**, 43-49.

White, A. B., C.W. Fairall, and D.W. Thomson, 1991: Radar Observations of Humidity Variability in and above the Marine Atmospheric Boundary Layer. *Journal of Atmospheric and Oceanic Technology*, **8**, 639-658.

Wyngaard, J.C., and M.A. LeMone, 1980: Behavior of the Refractive Index Structure Parameter in the Entraining Convective Boundary Layer. *Journal of Atmospheric Sciences*, **35**, 1573-1585.